Inorganic Chemistry

pubs.acs.org/IC

Featured Article

Resolving a Half-Century-Long Controversy between (Magneto)optical and EPR Spectra of Single-Electron-Reduced $[PcFe]^{-}$, $[PcFeL]^{-}$, and $[PcFeX]^{2-}$ Complexes: Story of a Double Flip

Briana R. Schrage,[‖] Wen Zhou,[‖] Laurel A. Harrison, Dustin E. Nevonen, John R. Thompson, Kathleen E. Prosser, Charles J. Walsby, Christopher J. Ziegler, Daniel B. Leznoff,* and Victor N. Nemykin*

Cite This: *Inorg. Chem.* 2022, 61, 20177−20199

Read Online

ACCESS | Metrics & More | Article Recommendations | Supporting Information

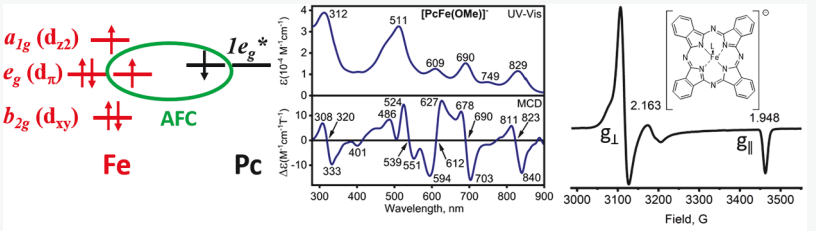

ABSTRACT: The reduction of iron(II) phthalocyanine ($Pc(2-)Fe^{II}$) or its bisaxially coordinated complexes results in the formation of the purple/red $[PcFe]^{-}$, $[PcFeL]^{-}$, and $[PcFeX]^{2-}$ (L is neutral and X is anionic ligand) species. The X-ray structure of the $[K(DME)_4][PcFe]$ complex exhibits a square-planar $[PcFe]^{-}$ anion. ^{1}H NMR spectra of the reduced species have one or two phthalocyanine broad peaks between 15 and 17 ppm. Solution magnetic moments are consistent with the presence of a single unpaired electron. A solid-state Mössbauer spectrum of $[K(DME)_4][PcFe]$ is consistent with an early report [Taube, R. *Pure Appl. Chem.***1974**, *38*, 427−438]. The solid-state EPR spectrum of the $[PcFe]^{-}$ anion is close to that recorded by Konarev et al. [*Dalton Trans.***2012**, *41*, 13841−13847]. Solution EPR spectra of reduced species have axial symmetry ($g_\perp \sim 2.08-2.17$ and $g_\parallel \sim 1.95-1.96$) and correlate well with spectra reported by Lever and Wilshire in 1978 [*Inorg. Chem.***1978**, *17*, 1145−1151]. The UV−vis spectra of pentacoordinated $[PcFeL]^{-}$ and $[PcFeX]^{2-}$ anions consist of the characteristic bands around 810, 690, and 515 nm. These bands correlate well with the set of MCD pseudo *A*-terms and resemble transitions in the $[Pc(3-)M]^{-}$ and $[Pc(3-)ML]^{-}$ compounds. The UV−vis and MCD spectra of $[PcFeL]^{-}$ and $[PcFeX]^{2-}$ complexes are in stark contrast to the crystallographically characterized reference $[Pc(2-)Co^{I}]^{-}$ anion, which is EPR silent, has a regular diamagnetic ^{1}H NMR spectrum, and has an intense Q-band at 699 nm, which correlates well with the strong MCD *A*-term. The DFT and TDDFT calculations are suggestive of the iron(II) center in a $(d_{xy})^2(d_{xz,yz})^3(d_{z^2})^1$ (s = 1) electronic configuration that is antiferromagnetically coupled with the one-electron-reduced Pc(3−) ligand (i.e., $[Pc(3-)Fe^{II}]^{-}$, $[Pc(3-)Fe^{II}L]^{-}$, and $[Pc(3-)Fe^{II}X]^{2-}$). The calculated EPR, Mössbauer, and UV−vis spectra of $[PcFe]^{-}$, $[PcFeL]^{-}$, and $[PcFeX]^{2-}$ complexes are in excellent agreement with the experimental data, thus resolving the controversy between axial s = 1/2 like EPR and Pc(3−)-like UV−vis spectra of these compounds.

INTRODUCTION

Iron phthalocyanine and its analogues accommodate a variety of oxidation states that span between +1 and +4 as well as spin states that vary between 0 and 5/2.[1−7] Such an ability to adopt a variety of oxidation and spin states that are supplemented by the affinity for coordination by a variety of axial ligands was exploited in the usage of these complexes for oxidative C−H bond activation in homogeneous and heterogeneous catalysis,[5,8−18] colorimetric detection of NO_x species and carbon monoxide,[9−23] electrocatalytic transformation of small molecules,[24−26] formation of the reactive oxygen species activators in cancer multidrug therapies,[27,28] and nanoscale electrode materials in the electrochemical detection of small biologically relevant molecules.[29−32] Iron(II) phthalocyanines tend to form low-spin diamagnetic hexacoordinate complexes with N-donors,[33−54] P-donors,[33,55−59] C-donors,[60−69] and S-donors,[70−72] while O-donors typically form PcFeL′L″ complexes with the sixth ligand being CO. Iron(III) phthalocyanines form both penta- and hexacoordinated monomeric or dimeric compounds depending on the type of axial ligand(s).[2,3,6,73−77] These complexes can adopt low-spin (s = 1/2), spin-admixed (s

Received: September 28, 2022
Published: December 6, 2022

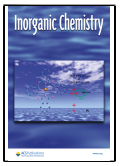

https://doi.org/10.1021/acs.inorgchem.2c03456
Inorg. Chem. 2022, 61, 20177−20199

= 3/5−5/2), and high-spin (s = 5/2) configurations. Both iron(II) and iron(III) phthalocyanines have been well-studied by a variety of spectroscopic (e.g., UV−vis, MCD, NMR, EPR, and Mössbauer) methods, and many of these compounds were also structurally characterized by X-ray crystallography.

On the other hand, information on the species that are formed upon reduction of tetra- and hexacoordinated iron(II) phthalocyanines remains scarce. In the 1960s and 1970s, several key reports on the nature of such reduced species were published. In 1972, Clack and Yandle reported the UV−vis spectrum of iron phthalocyanine reduced by sodium metal.[78] These authors noted that they were not able to observe the EPR spectrum for the red-colored reduced species.[79] In 1974, Taube reported Mössbauer spectra and magnetic properties on a single-electron-reduced iron phthalocyanine.[4] Finally, in 1978, Lever and Wilshire reported a UV−vis spectrum and a well-resolved solution EPR spectrum of a single-electron-reduced iron phthalocyanine.[71] The presence of an axial EPR signal with $g_{\perp}$ observed between 2.077 and 2.119 and $g_{\parallel}$ observed between 1.953 and 1.961 was interpreted as attributable to the formation of iron(I) complexes. Based on the superhyperfine splitting of the $g_{\parallel}$ signal observed for $[PcFeL]^-$ complexes with imidazole, pyridine, and triphenylphosphine axial ligands, it was concluded that a single-electron-reduced species had a $[Pc(2-)Fe^{I}L]^-$ formula (L = pyridine, imidazole, PPh_3, and DMA), with a d^7 iron(I) center located in a square-pyramidal environment. Lever and Wilshire also stated that the intense peak observed in the UV−vis spectrum of the reduced species at 516 nm is consistent with a Pc radical anion (i.e., not with an Fe(I)-containing species) but that "perturbation of the conventional Pc spectrum by low-valency metal ions to induce similar shifts" may also be possible.[71] Since that time, Lever's interpretation of the metal-centered one-electron-reduced iron(II) phthalocyanines has remained undisputed,[80−88] although Kobayashi and co-workers commented on the unusual spectrum of such a compound because it closely resembles the UV−vis spectra of one-electron-reduced main-group phthalocyanines of the general formula $[Pc(3-)M^{II}]^-$ and $[Pc(3-)M^{II}L]^-$ and thus "this profile can be easily misinterpreted as a reduction centered on the Pc ring".[89] Konarev and coauthors observed an additional band around 1050 nm in the samples of $[PcFeL]^-$ compounds, which they attributed to the radical nature of the phthalocyanine ligand.[88] However, these spectra were studied in the solid state, and thus aggregation-induced dimers or oligomers (similar to those observed in $([Pc(1-)M^{II}]_2^{\bullet+}$) can complicate the interpretation of the experimental data.[90]

X-ray data on one-electron-reduced iron(II) phthalocyanine complexes were extensively reported by Konarev and co-workers. Structural information on reduced PcFe complexes include materials with the formulas $[K([2.2.2]$-cryptand$)]^+[PcFe]^-$ (and the related sodium salt)[88] and $[Li_2(THF)(18\text{-crown-}6)_2]^+[PcFe]^-$ (THF = tetrahydrofuran),[91] [*N*,*N*,*N*-trimethylpiperazinium]$^+[PcFe]^-$,[87] and several materials that utilize reduced $[PcFe]^-$ anions as spin-bearing units in ternary materials, e.g. with fullerenes,[88,92] tryptycene, and *N*,*N*,*N*′,*N*′-tetrabenzyl-*p*-phenylenediamine,[86] and $[Cp^*_2Cr]$ cations.[93] Solid-state magnetometry data reported by Konarev and co-workers are indicative of an s = 1/2 ground state for single-electron-reduced iron(II) phthalocyanine species. The solid-state EPR spectra reported by Konarev and coauthors have strong counterion dependency and can be deconvoluted to several overlapping broad bands.[85−88] These EPR spectra are drastically different from the solution-phase EPR spectra reported by Lever and Wilshire in 1978[71] and more recently by Dzilinski and coauthors;[94] however, this is not surprising given the large observed differences in solid state and solution.

The main unresolved problem in the electronic structure of the single-electron-reduced iron(II) phthalocyanines is the discrepancy between the observed axial symmetry d^7-type (s = 1/2) EPR spectra of these species (which requires one-electron reduction of the iron(II) center) in solution and the phthalocyanine anion radical like UV−vis spectra (which requires one-electron reduction of the phthalocyanine ligand to form the organic radical anion). Our interest in single-electron-reduced iron(II) phthalocyanines converged from two directions. First, we are interested in generating and isolating reduced PcM species using chemical reducing agents.[95−97] Thus, in continuation of our studies on the isolated single-electron-reduced phthalocyanine species, we have studied the reduction and isolation of iron(II) phthalocyanine derivatives. Second, we recently discussed the b_{1u}*−b_{2u}* energy gap in $PcFeL_2$, PcFeL′L″, or $[PcFeX_2]^{2-}$ complexes (Figure 1), which,

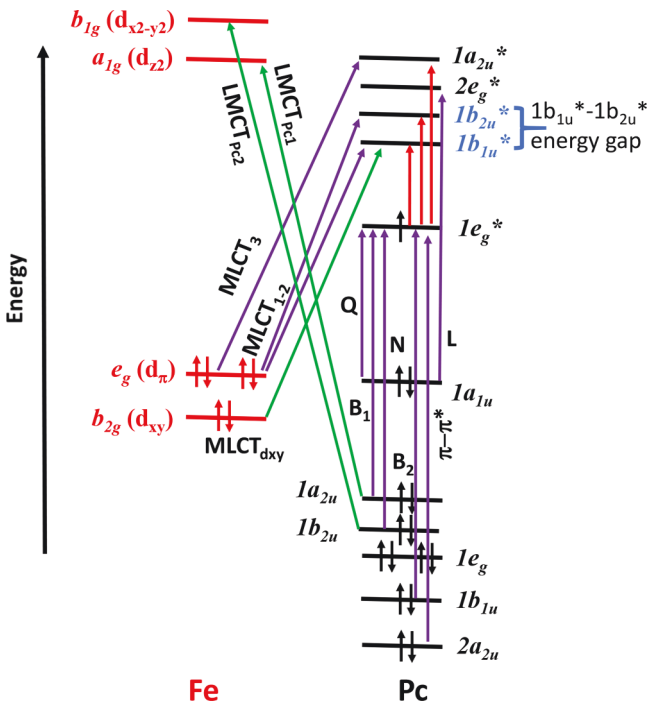

Figure 1. Hypothetical arbitrary energy molecular diagram for the ^2E_g ground state of a $[Pc(3-)Fe^{II}L]^-$ complex with a low-spin iron center. Vertical arrows are associated with the symmetry allowed (in a standard for phthalocyanine D_{4h} point group) metal-to-ligand charge transfer (MLCT), ligand-to-metal charge transfer (LMCT), and phthalocyanine-centered transitions. Red arrows indicate transitions that originate from the reduced $1e_g$* MOs. Violet and red arrows represent *XY*-polarized transitions, and green arrows represent *Z*-polarized transitions.

based on magnetic circular dichroism (MCD) and time dependent density functional theory (TDDFT) data, should be around 0.10−0.15 eV.[98] Similar to main-group phthalocyanines of the general formula $[Pc(3-)M^{II}]^-$ (M = Mg or Zn),[99−101] we speculated that this gap can be directly measured using MCD spectra of $[Pc(3-)Fe^{II}L_n]^-$ (n = 1 or 2) complexes as $7e_g$* → $1b_{1u}$*/$1b_{2u}$* transitions should be observable in the 500−600 nm region, assuming that the first reduction of the

https://doi.org/10.1021/acs.inorgchem.2c03456
Inorg. Chem. 2022, 61, 20177−20199

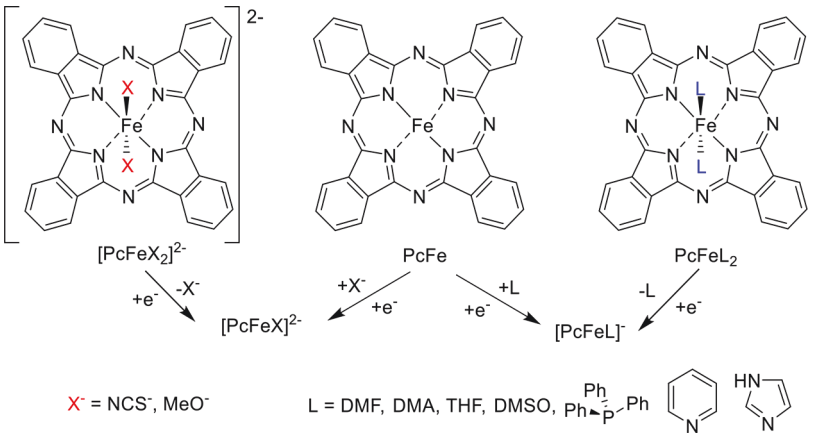

Figure 2. Generation and structures of the reduced species discussed in this paper.

Table 1. Summary of Crystallographic Data for 1 and 2

	1	2
empirical formula	$C_{48}H_{56}N_8O_8KFe$	$C_{48}H_{56}N_8O_8KCo$
formula weight	967.95	971.04
temperature (K)	150(2)	150(2)
crystal system	monoclinic	monoclinic
space group	*Cm*	*Cm*
a (Å)	16.8604(16)	16.584(8)
b (Å)	38.787(3)	38.673(19)
c (Å)	12.3645(11)	12.272(6)
α (deg)	90	90
β (deg)	110.426(2)	109.743(12)
γ (deg)	90	90
volume (Å^3)	7577.5(12)	7408(6)
Z	4	4
ρ_{calc} (g/cm^3)	1.251	1.270
μ (mm^{-1})	0.437	0.489
F(000)	2966.0	2951.0
crystal size (mm^3)	1.08 × 0.3 × 0.08	0.513 × 0.286 × 0.157
radiation	Mo Kα (λ = 0.71073)	Mo Kα (λ = 0.71073)
2Θ range for data collection (deg)	2.784−50.046	3.76−50.054
reflections collected	60043	22425
independent reflections	13609 [R_{int} = 0.0397, R_{sigma} = 0.0368]	10954 [R_{int} = 0.0420, R_{sigma} = 0.0586]
data/restraints/parameters	13609/91/960	10954/117/922
goodness of fit on F^2	1.341	1.239
final *R* indexes [$I \geq 2\sigma(I)$]	R_1 = 0.0653, wR_2 = 0.1665	R_1 = 0.0728, wR_2 = 0.1879
final *R* indexes [all data]	R_1 = 0.0759, wR_2 = 0.1730	R_1 = 0.0878, wR_2 = 0.1967
largest diff peak/hole (e Å^{-3})	1.48/−0.68	1.10/−1.09
Flack parameter	0.41(2)	0.47(3)

PcFe, $PcFeL_2$, and $[PcFeX_2]^{2-}$ species is phthalocyanine-centered.

In order to address the two aforementioned questions and resolve the spectroscopy-based conundrum for the $[PcFe]^-$, $[PcFeL]^-$, and $[PcFeX]^{2-}$ complexes, we have reduced a number of iron(II) phthalocyanine compounds with different axial ligands (Figure 2) as well as the parent unligated PcFe and have analyzed their electronic structures using UV−vis, MCD, solution EPR, density functional theory (DFT), and TDDFT methods. In addition, we also were able to crystallize the four-coordinate $[PcFe]^-$ anion and obtain its solid-state Mössbauer and EPR spectra. We compared data on single-electron-reduced iron phthalocyanine species with similar data for the cobalt complex. As we will demonstrate below, our analysis explains all of the inconsistencies in the spectroscopic data observed for these compounds and confirms the low-energy gap between $1b_{1u}$* and $1b_{2u}$* unoccupied orbitals in iron phthalocyanines.

RESULTS AND DISCUSSION

Isolation and Structures of Single-Electron-Reduced Iron(II) and Cobalt(II) Phthalocyanines. In order to generate redox-active species in solution, iron(II) phthalocyanine and its bisaxial adducts can be reduced under chemical or bulk electrolysis conditions (Figure 2). Both approaches were used earlier by several research groups.[4,71,78,81−89,94] In the case of the chemical reduction, the parent iron(II) phthalocyanine was reduced by lithium[4] or sodium[78] metal in THF or dimethoxyethane (DME) solutions. As we will show below, in THF solution, this reduction results in the formation of the $[PcFe(THF)]^-$ complex, while based on our data shown

https://doi.org/10.1021/acs.inorgchem.2c03456
Inorg. Chem. 2022, 61, 20177−20199

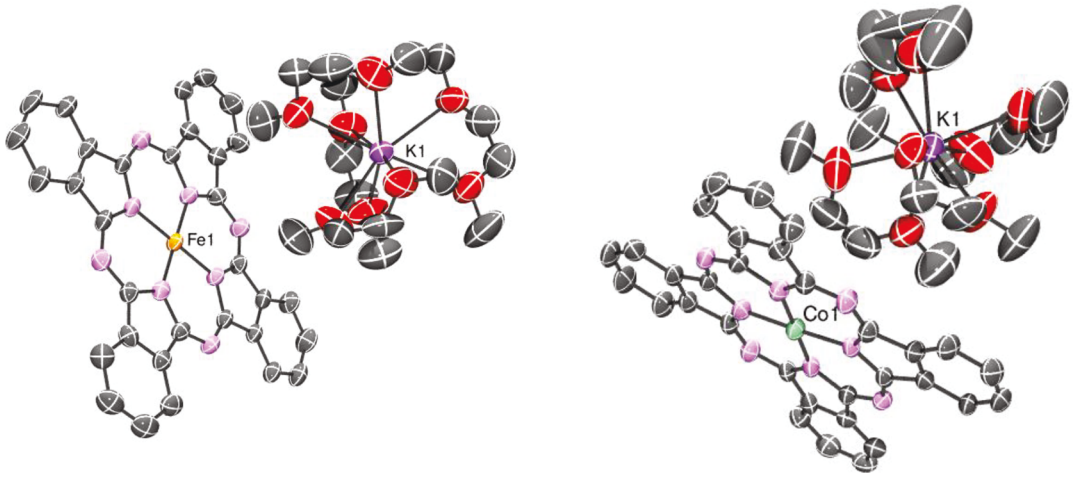

Figure 3. Molecular structure of $[K(DME)_4][PcFe]$ (**1**, left) and $[K(DME)_4][PcCo]$ (**2**, right). Thermal ellipsoids are set at 30% probability. Hydrogen atoms have been omitted for clarity.

below, no axial coordination occurred in dry DME solution. In addition, the chemical reduction of iron(II) phthalocyanine can be achieved in a mixture of (i) MeOH, NaOH, and $NaBH_4$; (ii) $NaBH_4$ and a coordinating solvent; and (iii) $KBEt_3H$ and a coordinating solvent or DME (which does not coordinate to the iron center). As we will show below, the first approach leads to the formation of the $[PcFe(OMe)]^{2-}$ complex. The second and third approaches have a broader scope and allow for the generation of $[PcFeL]^-$ and $[PcFeX]^{2-}$ anions in solution (L is a neutral ligand and X^- is a monoanionic axial ligand). Because of the solubility of $KBEt_3H$ in polar organic solvents, the reduction of the iron(II) complexes with this reagent can be easily monitored by UV−vis spectroscopy. However, in our hands, the heterogeneous reduction reaction with $NaBH_4$ always resulted in the clean formation of one-electron-reduced species, while use of an excess $KBEt_3H$ can lead (in some cases) to the formation of one- and two-electron-reduced complexes. The second general approach to generate reduced iron(II) phthalocyanine species was explored by Lever and Wilshire.[71] This method includes bulk electrolysis of the bisaxially coordinated iron(II) phthalocyanine, sometimes in the presence of an additional axial ligand (present at the beginning of the electrolysis or added after the electrolysis is complete). As we will show below, both chemical and electrochemical reductions in our hands result in the formation of the reduced species with the same spectroscopic signatures.

With respect to the third synthetic methodology, the addition of 1 equiv of potassium triethylborohydride (as a solution in THF) to a suspension of PcM (M = Fe, Co) in DME in rigorously dry and oxygen-free conditions resulted in the immediate solublization of the PcM starting material and an accompanying color change from blue to dark purple for M = Fe and from blue to yellow/green for M = Co. Filtration of the reaction mixture and evaporation of the solvent yielded purple $[K(DME)_4][PcFe]$ (**1**) and a green $[K(DME)_4][PcCo]$ (**2**) powders in good yields. These materials are extremely air and moisture sensitive, precluding any analysis by MALDI-TOF or other mass spectroscopy, although elemental analysis (C, H, N) is consistent with the proposed formulas (subject to a small amount of DME loss). Very air-sensitive X-ray quality crystals of **1** and **2** were obtained via layering and slow diffusion of hexanes into concentrated DME solutions.

The structures of **1** and **2** are isomorphous, with very similar unit cells (Table 1), containing two crystallographically independent (but structurally very similar) $[K(DME)_4]^+$ cations and two unsolvated, four-coordinate $[PcM]^-$ anions.

Each structure contains a potassium cation coordinated by four DME molecules ($[K(DME)_4]^+$), clearly separated and noninteracting with the anion $[PcM]^-$, which has a rigidly square-planar M center within the plane of the Pc ligand (Figure 3); no axial ligands are present in either structure. The M−N bond lengths of Co−N 1.899(6)−1.917(7) Å in **2** (Table 2 and Table S1) can be compared with the Co−N distances of 1.906(2) and 1.909(2) Å in PcCo[102] and 1.88(1)−1.92(1) Å in $[nBu_4N][PcCo^I]$.[103] For Fe-containing compound **1**, the Fe−N bond lengths of 1.906(5)−1.923(5) Å can be compared with bond lengths of 1.927(1) Å in PcFe,[104] 1.938(2) Å in diamagnetic $PcFe(pyridine)_2$[105] and 1.910(3)−1.9252(13) Å in a series of reduced $[PcFe(I)]^-$ anions;[88] both of the PcM structures were collected at room temperature while the data reported herein were obtained at 150 K, and thus the observed small shortening of the bond lengths (in the [PcM] anions relative to the PcM data) can be expected. Changes in M−N bond lengths are not, in this case, significantly sensitive to the metal oxidation state, although the M−Npc bond lengths do show a larger variation compared to cases where axial ligands are bound. The Pc ligand is only distorted from planarity between 0 and ∼12.5° in **2** (based on planes defined by adjacent isoindolene rings) and between 0 and ∼9.1° in **1**; in both cases most adjacent planes are under 3° and thus the Pc rings are generally very flat.

Table 2. Selected Bond Lengths (Å) for 1 and 2

bond	**1** (M = Fe)	**2** (M = Co)
M−N(1)	1.923(5)	1.906(6)
M−N(3)	1.917(5)	1.917(7)
M−N(5)	1.906(5)	1.899(6)
M−N(7)	1.921(5)	1.901(7)

Reduction of the aromatic 18-π-electron circuit of the Pc ligand often generates a disruption of the aromaticity, manifesting in localizing alternating short and long bonds around the Pc ligand; this is readily observed in doubly reduced Pc(4−) systems[106−108] but often much less so in monoreduced

https://doi.org/10.1021/acs.inorgchem.2c03456
Inorg. Chem. 2022, 61, 20177−20199

Table 3. Reduction Potentials of $PcFeL_2$ and $[PcFeX_2]^{2-}$ Complexes[a]

complex	solvent	electrolyte[b]	Red_1	Red_2	ref[c]
$PcFePy_2$	Py	TEAP	−1.07	−1.32	71
	Py	TBAP	−1.07	−1.32	tw
	Py	?	−1.09	−1.39	111
	DMSO/1 M Py	TBAP	−0.95	−1.22	80
	DMSO/5% Py	TBAP	−0.93	−1.19	tw
	DMF/5% Py	TBAP	−0.97	−1.27	112
	DCM/5% Py	TBAP	−1.08		112
$PcFeIm_2$	DMSO/1 M Im	TBAP	−1.21[d]		80
	DMSO/0.01 M Im	TBAP	−1.02	−1.15	80
	DMF/Im	TBAP	−1.14	−1.74	tw
$PcFe(DMSO)_2$	DMSO	TBAP	−0.74	−1.15	80
	DMSO	TBAP	−0.72	−1.15	tw
	DMSO	TEAP	−0.71	−1.15	71
$PcFe(DMSO)_2$	$DMSO/PPh_3$	TBAP	−0.71	−1.14	tw
$PcFe(DMA)_2$	DMA	TEAP	−0.55	−1.17	71
	DMA	TBAP	−0.91[e]	−1.14	71
$PcFe(DMF)_2$	DMF	TPAP	−1.56	−2.05	113
$[PcFe(NCS)_2]^{2-}$	DMF	KNCS	−1.11	−1.58	tw
$[PcFe(OMe)_2]^{2-}$	DMF/MeOH	TBAP/NaOH	−1.56	−2.19	tw
$[PcFe(OMe)_2]^{2-}$	MeOH	TBAP/NaOH	−1.37 (irr)		tw

[a]All potentials are given versus SCE. Formulas for the initial $PcFeL_2$ complexes are listed in the first column. [b]TEAP = tetraethylammonium perchlorate; TBAP = tetrabutylammonium perchlorate; TPAP = tetrapropylammonium perchlorate. [c]tw = this work. [d]Two-electron process. [e]Dropping mercury electrode data.

Pc(3−) systems. For example, the monoreduced $Al^{III}Pc^{3-}(anisole)_2$[109] contains a nearly flat Pc ring with delocalized bonds, with the largest dihedral angle between the C_8N_8 mean plane and an isoindole moiety of ∼3.8°; the PcMg(3−) complex is similar.[95] First-row transition-metal Pc complexes with Pc(3−) species can show some bond-length alternation in the C−N imine bonds,[110] but there is no strong evidence for breaking of the aromaticity of the Pc ligand in the form of bond localization in either **1** or **2**, consistent with previous reports of other reduced PcFe- and PcCo-containing systems.

Electrochemistry and Spectroscopy of Single-Electron-Reduced Iron(II) and Cobalt(II) Phthalocyanines. Electrochemical reduction potentials for axially coordinated iron(II) phthalocyanine are listed in Table 3 with a representative example shown in Figure 4. Similar to previous reports,[71,80] two reduction processes were generally observed. As was proven by Lever's and Kadish's research groups,[71,80] even when reduction waves observed in cyclic voltammetry (CV) experiments appear reversible, the first reduction process reflects the axial ligand dissociation process shown in eq 1:

$$PcFeL_2 + e^- \rightleftharpoons [PcFeL]^- + L \quad (1)$$

Another interesting observation is that the reduction potentials of the $PcFe(DMSO)_2$ complex in neat DMSO and in DMSO in the presence of PPh_3 are virtually the same, while the EPR, UV−vis, and MCD spectra of the single-electron-reduced species are different. This is indicative of axial coordination of DMSO and PPh_3 to the reduced species, respectively. This could be reflective of the following equilibria:

$$PcFe(DMSO)_2 + e^- \rightleftharpoons [PcFe(DMSO)]^- + DMSO \quad (2)$$

$$[PcFe(DMSO)]^- + PPh_3 \rightleftharpoons [PcFe(PPh_3)]^- + DMSO \quad (3)$$

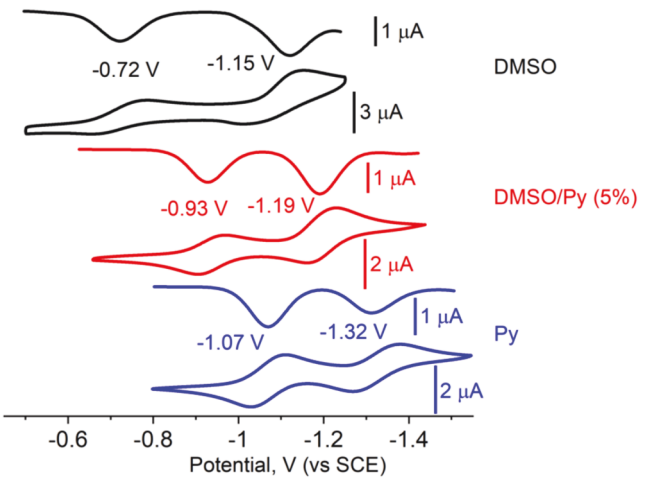

Figure 4. Representative examples of the electrochemistry of $PcFeL_2$ complexes. Black, $PcFe(DMSO)_2$ in DMSO/0.1 M TBAP; red, same complex in DMSO/Py (95:5 v:v) mixture with 0.1 M TBAP; blue, $PcFePy_2$ in Py/0.1 M TBAP.

The transformations outlined in eqs 2 and 3 are not unique. Indeed, in 1978 Kadish and co-workers already observed very close reduction potentials for the $PcFe(DMSO)_2$ complex in neat DMSO and DMSO/1 M Py^R mixtures (Py^R = 2,6-lutidine, 2,4-lutidine, and 2,4,6-collidine).[80] Next, we have studied the reversibility of the reduction process under spectroelectrochemical conditions to ensure that the experimental spectroscopic signatures do not belong to degradation products (Figure 5 and Figures S7−S17). In all cases, reduction of the iron(II) phthalocyanines of general formulas $PcFeL_2$ and $[PcFeX_2]^{2-}$ under spectroelectrochemical conditions results in the disappearance of the Q-band observed between 650 and 655 nm and $MLCT_{1-2}$ transitions observed between 410 and 460 nm, as well as the appearance of the bands at ∼810, ∼690, ∼600, and

https://doi.org/10.1021/acs.inorgchem.2c03456
Inorg. Chem. 2022, 61, 20177−20199

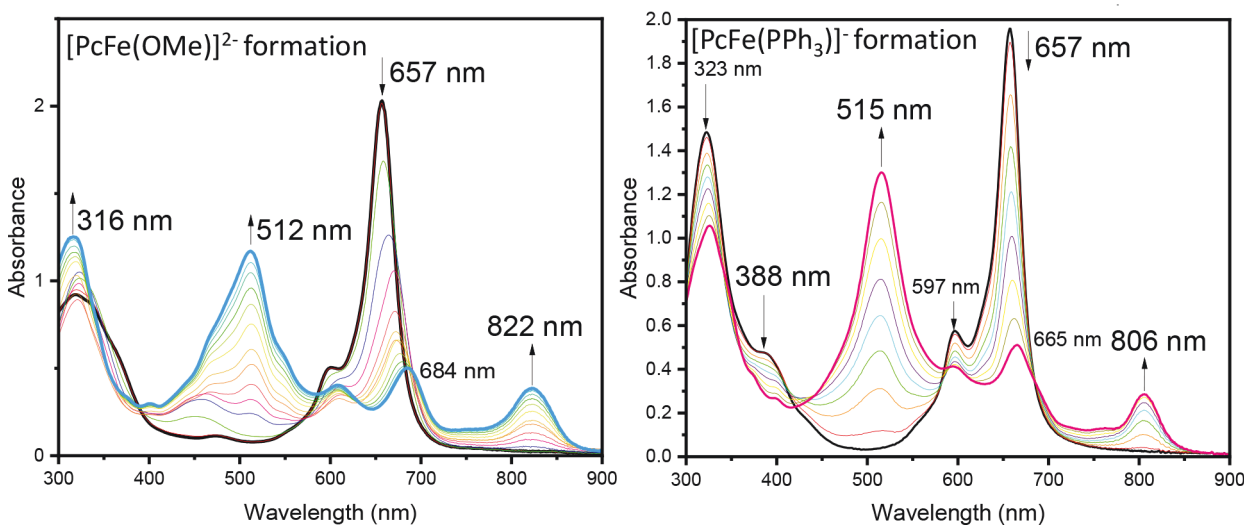

Figure 5. Formation of $[PcFe(OMe)]^{2-}$ (left) and $[PcFe(PPh_3)]^{-}$ (right) species under spectroelectrochemical conditions in the DMF/0.3 M TBAP system.

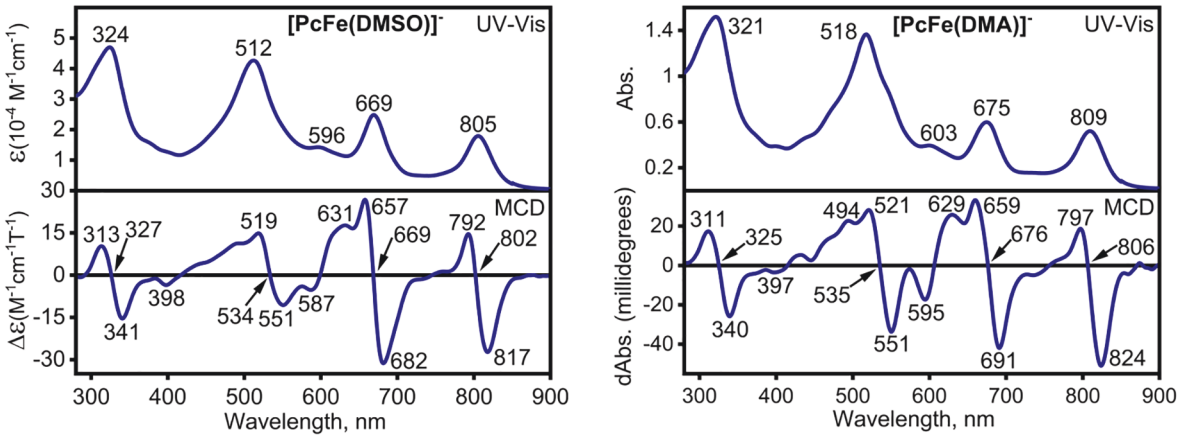

Figure 6. Representative examples of UV−vis and MCD spectra of $[PcFeL]^{-}$ complexes. See the Supporting Information for all other compounds.

~515 nm. The last band dominates the spectrum. The spectral transformations have some axial ligand dependency. For instance, the lowest energy band was observed between 809 and 829 nm, while the main transition at ~515 nm developed visible shoulders when DMA, NCS^{-}, Im, and MeO^{-} were used as the axial ligands (Figure 5). The reduced $[PcFeL]^{-}$ and $[PcFeX]^{2-}$ complexes have very high affinity for axial ligands, which is evident from the EPR spectra discussed below. Indeed, DMF, DMA, THF, and PPh_3 axial ligands have very weak affinity toward the parent unreduced iron(II) phthalocyanine. However, Lever's[71] and our UV−vis, MCD, and EPR data are clearly indicative of the axial coordination of these molecules to the iron center. All reduced $[PcFeL]^{-}$ and $[PcFeX]^{2-}$ complexes can be reoxidized back to the initial $PcFe^{II}L_2$ and $[PcFe^{II}X_2]^{2-}$ compounds with 80−90% yield under spectroelectrochemical conditions (Figures S7−S17). It is interesting to note that the PPh_3 ligand in $[PcFe(PPh_3)]^{-}$ gets exchanged with DMSO molecules during the reoxidation reaction as the final spectrum is indistinguishable from the $PcFe(DMSO)_2$ complex but the resultant spectrum is very different from the UV−vis spectra of $PcFe(PR_3)_2$ compounds.[98]

Since it is difficult to achieve complete reduction of the $PcFe^{II}L_2$ and $[PcFe^{II}X_2]^{2-}$ complexes and because of the difficulties in collecting MCD spectra of the reduced $[PcFeL]^{-}$ and $[PcFeX]^{2-}$ compounds generated under spectroelectrochemical conditions, we also explored chemical reduction protocols for all target compounds. Out of two approaches we tried (reduction with sodium metal and reduction by $NaBH_4$ or $KBEt_3H$), the more reliable synthetic protocol involves reduction with $NaBH_4$ (see the Experimental Section for details), which allowed us to investigate MCD spectra of the reduced species in detail (Figure 6). Again, the UV−vis spectra of the purple $[PcFeL]^{-}$ and $[PcFeX]^{2-}$ complexes obtained under spectroelectrochemical and chemical reduction conditions are indistinguishable from each other. The spectra do not change significantly between room temperature and −55 °C (Figure 7). They have some axial ligand dependency and differ significantly from the UV−vis spectra that involve the traditional blue or green Pc(2−) chromophore. In fact, the UV−vis spectra of reduced $[PcFeL]^{-}$ and $[PcFeX]^{2-}$ complexes closely resemble the UV−vis spectra of $[Pc(3-)M^{II}]^{-}$ and $[Pc(3-)M^{II}L]^{-}$ (M = Mg or Zn) species reported by several research groups.[99−101] The lowest energy band was observed between 805 and 829 nm (ΔE = 360 cm^{-1}). No transitions were detected between 850 and 2500 nm, which confirms our hypothesis that the solid-state UV−vis spectra reported by Konarev and coworkers also reflect aggregation between phthalocyanine monomers.[88] One key difference between the UV−vis spectra

https://doi.org/10.1021/acs.inorgchem.2c03456
Inorg. Chem. 2022, 61, 20177−20199

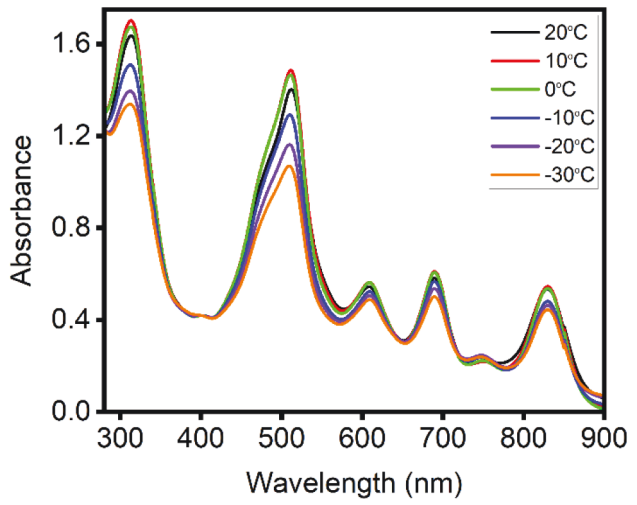

Figure 7. Variable-temperature UV−vis spectra of $[PcFe(NCS)]^{2-}$ in DMF.

of pentacoordinate $[PcFeL]^-$ and $[PcFeX]^{2-}$ and tetracoordinate $[PcFe]^-$ complexes is the significant reduction of the intensity of the band at ∼690 nm. Indeed, the UV−vis spectrum of the isolated $[PcFe]^-$ complex recorded in dry DME inside the drybox (Figure 8) has a band at ∼690 nm with low intensity,

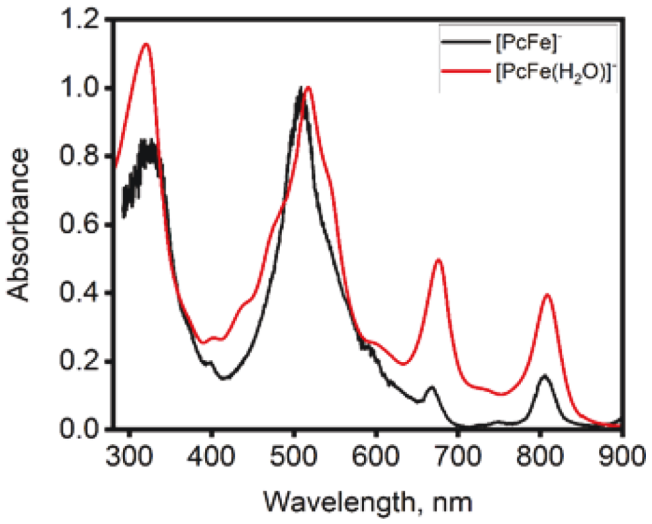

Figure 8. Comparative UV−vis spectra of $[PcFe]^-$ recorded in dry (black) and wet (red) DME.

while the UV−vis spectrum of the PcFe reduced with $NaBH_4$ in wet DME has this transition at higher intensity and closely resembles the UV−vis spectra of $[PcFeL]^-$ and $[PcFeX]^{2-}$ complexes, which probably reflects the formation of the $[PcFe(H_2O)]^-$ complex (Figure 8). The axial ligand dependency of this band can be clearly seen, as its position varies between 661 and 690 nm (ΔE = 640 cm^{-1}). This band is always red shifted compared to the Q-band position in the initial $PcFeL_2$ or $[PcFeX_2]^{2-}$ complexes. A smaller intensity band at 596−609 nm was also observed in the UV−vis spectra of $[PcFeL]^-$ and $[PcFeX]^{2-}$. The next most intense absorption band is observed between 511 and 518 nm. This band produces the purple/red color of the reduced species and typically has shoulders at lower- and higher-energy regions. Finally, the Soret-like absorption band was observed around 320 nm in all reduced compounds. Overall, the UV−vis spectral profile observed for our pentacoordinate compounds is in excellent agreement with the spectra reported by Lever and Wilshire in 1978[71] and Dzilinski and coauthors in 2007.[94] The UV−vis spectrum of the tetracoordinate $[PcFe]^-$ anion has a significantly more intense band at 512 nm and a less intense ∼690 nm transition compared to the pentacoordinate species. In excellent agreement with Lever and Wilshire's data,[71] the molar extinction coefficients for all absorption bands in the 400−850 nm spectral envelope are significantly reduced (by at least 4 times) compared to the intensity of the Q-band in the parent $PcFeL_2$ and $[PcFeX_2]^{2-}$ complexes[98] and a similar trend was observed for all reduced ring-substituted iron phthalocyanines reported to date. In contrast, only a slight red shift of the Q-band was observed upon reduction of PcCo (Figure 9). The diamagnetic $[Pc(2-)Co^{I}]^-$ complex has a UV−vis spectrum expected for a Pc(2−)-containing phthalocyanine compound. In particular, the intensities of the Q-bands in $Pc(2-)Co^{II}$ and $[Pc(2-)Co^{I}]^-$ complexes are close to each other ($\varepsilon \sim 10^5$ M^{-1} cm^{-1}),[114,115] supporting the presence of a Pc(2−) macrocycle in both compounds. On the other hand, the UV−vis spectra of $[PcFe]^-$, $[PcFeL]^-$, and $[PcFeX]^{2-}$ complexes are not characteristic of the presence of the Pc(2−) ligand and instead resemble spectra of the Pc(3−) chromophore.[95−97,99−101]

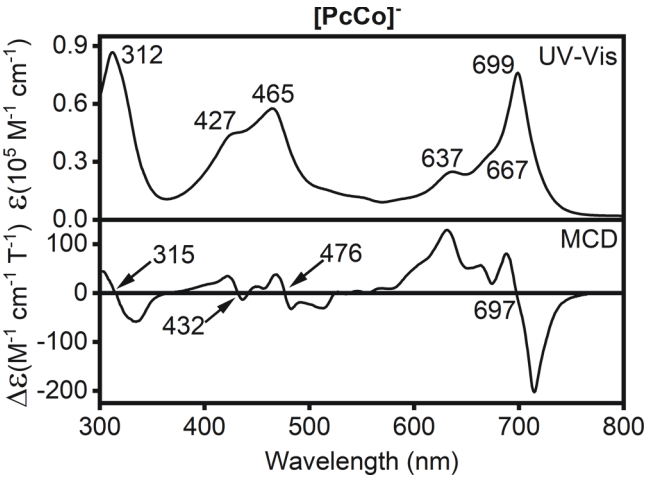

Figure 9. UV−vis and MCD spectra of $[Pc(2-)Co^{I}]$ in DMF.

The MCD spectra of $[PcFeL]^-$ and $[PcFeX]^{2-}$ complexes are very rich and consist of several clearly visible MCD pseudo *A*-terms in the 300−900 nm region (Figure 6). For instance, in the case of $[PcFe(DMSO)]^-$, four pseudo *A*-terms centered at 802, 669, 534, and 327 nm have been observed and similar features were observed for all other compounds studied by MCD spectroscopy. As with the $[Pc(3-)M^{II}]^-$ (M = Mg or Zn) species reported by Stillman and co-workers,[99−101] one might expect that the addition of the electron to the previously unoccupied $7e_g$* orbitals of the phthalocyanine core will (i) lead to the static Jahn−Teller distortion and (ii) stabilize the $7e_g$* orbitals and thus decrease the energy of the Q-band (predominantly $1a_{1u} \rightarrow 7e_g$* single-electron excitation). Indeed, based on the MCD spectroscopy, Stillman and coauthors identified the Q-band in $[Pc(3-)M^{II}]^-$ (M = Mg or Zn) complexes around 930 nm and suggested that the Jahn−Teller effect for this band is small (∼300 cm^{-1}).[99−101] In the case of $[PcFeL]^-$ and $[PcFeX]^{2-}$ complexes, their MCD spectra are closer to those containing a Pc(3−) ligand than the regular

https://doi.org/10.1021/acs.inorgchem.2c03456
Inorg. Chem. 2022, 61, 20177−20199

Pc(2−) macrocycle (see discussion below). In general, each MCD spectrum has four Faraday pseudo *A*-terms centered around 780−800, 650−690, 535, and 320 nm (Figure 6 and Figures S18−S24). Pseudo *A*-terms centers correlate to some extent with the absorption peaks observed in the corresponding UV−vis spectra. For instance, the lowest energy MCD pseudo *A*-term is centered around 780−820 nm. The center of this pseudo *A*-term does correlate with the position of the prominent absorption band observed in the UV−vis spectra of the reduced species between 809 and 829 nm. Thus, similar to the analysis provided by Stillman and co-workers,[99−101] the low-energy MCD signal consists of two closely spaced *B*-terms of opposite amplitudes. The *B*-term with the negative amplitude correlates well with the position of the low-energy band observed in the UV−vis spectra of $[PcFeL]^-$ and $[PcFeX]^{2-}$ complexes. Similar to the $[Pc(3-)M^{II}]^-$ (M = Mg or Zn) complexes[99−101] and in agreement with our TDDFT calculations discussed below, this band was assigned as the Q-band and the small energy difference between negative and positive *B*-terms can be attributed to the static Jahn−Teller effect. The second Faraday pseudo *A*-term is centered between 650 and 690 nm. This pseudo *A*-term has an axial ligand dependency, and similar to the lowest energy pseudo *A*-term, its center correlates well with the position of the band in UV−vis spectra of $[PcFeL]^{2-}$ and $[PcFeX]^{2-}$ complexes. This band has a significantly lower intensity in the UV−vis spectrum of the $[PcFe]^-$ complex taken inside a drybox in DME (Figure 8). However, this band was observed by Lever and Wilshire in 1978[71] as well as Dzilinski and coauthors in 2007.[94] We speculate (and this agrees well with our TDDFT calculations discussed below) that this band is characteristic of pentacoordinated $[PcFeL]^-$ and $[PcFeX]^{2-}$ complexes and is forbidden in the four-coordinate $[PcFe]^-$ species. The third MCD pseudo *A*-term is located around the prominent absorption observed between 510 and 535 nm in the UV−vis spectra of the $[PcFeL]^-$ and $[PcFeX]^{2-}$ complexes (Figure 6 and Figures S18−S24). Unlike for the previous two pseudo *A*-terms, the energy of the positive amplitude *B*-term correlates with the center of the UV−vis band. Finally, the fourth MCD pseudo *A*-term is centered between 315 and 330 nm and its center correlates well with the position of the Soret-type band observed in the UV−vis spectra of the $[PcFeL]^-$ and $[PcFeX]^{2-}$ complexes.

The UV−vis and MCD spectra of $[PcCo]^-$ are very different from those observed for iron derivatives (Figure 9), and they correlate well with the data reported by Stillman and Thomson in 1974.[114,115] In particular, the red-shifted (compared to the parent PcCo) Q-band at 699 nm agrees well with a very intense MCD *A*-term, while the other MCD signals have significantly lower amplitudes, especially in the 300−550 nm spectral envelope. Such a discrepancy between the Q-band intensity and the 300−550 nm band intensities in the MCD spectra of closed-shell phthalocyanines is very characteristic for Pc(2−) chromophores. Thus, in agreement with the previous assignments,[89,114,115] the single-electron-reduced PcCo species can be formulated as a $[Pc(2-)Co^{I}]^-$ species, which also correlates well with their diamagnetic ^{1}H NMR spectra and lack of EPR signal. On the other hand, the overall profile of the UV−vis and MCD spectra of $[PcFe]^-$, $[PcFeL]^-$, and $[PcFeX]^{2-}$ complexes are reflective of the single-electron reduction of the phthalocyanine macrocycle rather than metal center. Thus, at first glance, the single-electron-reduced iron phthalocyanine derivatives can be formulated as $[Pc(3-)Fe^{II}]^-$, $[Pc(3-)Fe^{II}L]^-$, and $[Pc(3-)Fe^{II}X]^{2-}$ species.

Such an assignment, however, seemingly contradicts the solution EPR data published by Lever and Wilshire in 1978[71] and Dzilinski's group in 2007.[94] Indeed, unlike the solid-state EPR data on reduced $[PcFeL]^-$ and $[PcFeX]^{2-}$ complexes reported by Konarev and co-workers[85−88] as well as us (Figure S50), the solution EPR spectra of these species have clear axial symmetry and are seemingly reflective of the presence of an $s = 1/2$ system (Figure 10 and Figures S25−S31). Because of the

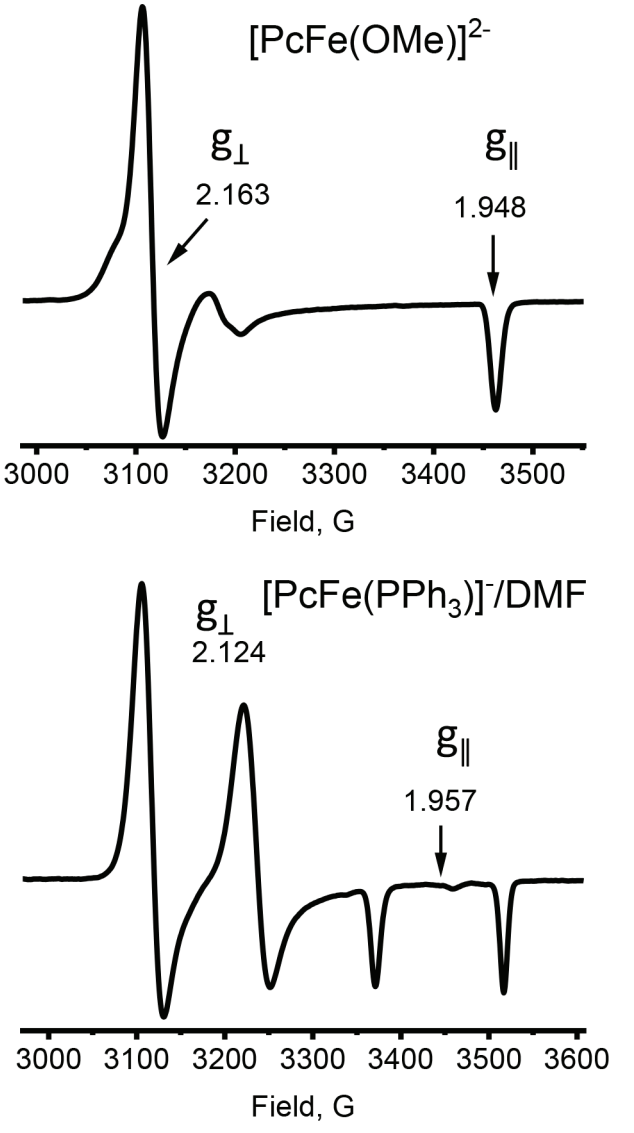

Figure 10. Representative examples of solution EPR spectra of $[PcFeL]^-$ and $[PcFeX]^{2-}$ complexes in frozen solutions at 77 K.

presence of the superhyperfine triplet in the EPR spectra of $[PcFeL]^-$ (L = Py or Im) and the superhyperfine doublet in the EPR spectrum of $[PcFe(PPh_3)]^-$, Lever and Wilshire reasonably concluded that the reduction process is iron centered and thus the $[PcFeL]^-$ and $[PcFeX]^{2-}$ complexes have pentacoordinate iron(I) d^7 centers with EPR-active $(d_{z^2})^1$ configuration and should be formulated as $[Pc(2-)Fe^{I}L]^-$.[71] Our frozen solution data on the $[PcFeL]^-$ and $[PcFeX]^{2-}$ complexes are in excellent agreement with the data reported by Lever and Wilshire and are indicative of the presence of an axial $s = 1/2$ system. We also would like to reiterate the high affinity of the iron centers in the $[PcFeL]^-$ and $[PcFeX]^{2-}$ complexes toward axial ligands.

https://doi.org/10.1021/acs.inorgchem.2c03456
Inorg. Chem. 2022, 61, 20177−20199

Table 4. Experimental and DFT-Predicted EPR Spectra Parameters in $[PcFe]^-$, $[PcFeL]^-$, and $[PcFeX]^{2-}$ Complexes

	experiment[a]					TPSSh (gas)				TPSSh (DMF)				revTPSS (DMF)			
complex	$g_\perp$	$g_\parallel$	A^b	solvent	ref[c]	g_1	g_2	g_3	A^b	g_1	g_2	g_3	A^b	g_1	g_2	g_3	A^b
$[PcFe]^-$	2.11	1.96		*d*	94	2.233	2.232	1.766		2.230	2.230	1.867		2.201	2.201	1.908	
$[PcFePy]^-$	2.119	1.956	13	*e*	71	2.164	2.149	1.870	12	2.165	2.150	1.864	12	2.124	2.119	1.903	15
$[PcFeIm]^-$	2.112	1.956	13	*f*	71	2.155	2.147	1.836	13	2.153	2.146	1.823	12	2.122	2.122	1.899	15
$[PcFe(NCS)]^{2-}$	2.170	1.953		*g*	tw	2.135	2.135	1.823	18	2.144	2.144	1.761	16	2.124	2.124	1.896	18
$[PcFe(PPh_3)]^-$	2.077	1.958	133	*h*	71	2.199	2.168	1.866	97	2.182	2.166	1.757	106	2.126	2.123	1.910	145
	2.118	1.959	147	*i*	tw												
	2.124	1.957	146	*j*	tw												
$[PcFe(OMe)]^{2-}$	2.163	1.948		*k*	tw	2.118	2.117	1.957		2.128	2.127	1.912		2.108	2.106	1.925	
$[PcFe(THF)]^-$	2.13	1.96		*l*	94	2.212	2.169	1.886		2.197	2.163	1.849		2.156	2.155	1.900	
	2.131	1.951		*m*	tw												
$[PcFe(DMF)]^-$	2.163	1.951		*n*	tw	2.201	2.166	1.890		2.163	2.163	1.754		2.148	2.147	1.900	
$[PcFe(DMA)]^-$	2.119	1.953		*o*	71												
	2.162	1.950		*p*	tw												
$[PcFe(DMSO)]^-$	2.077	1.961		*q*	71	2.191	2.163	1.874		2.189	2.162	1.866		2.126	2.123	1.910	
	2.099	1.957		*r*	tw												

[a]At 77 K unless specified. [b]A_{iso} in gauss. [c]tw = this work. [d]DME/Na. [e]In Py/LiCl, bulk electrolysis. [f]DMA/LiCl, Im added to $[PcFe]^-$ after bulk electrolysis. [g]DMF/$NaBH_4$. [h]DMSO/TBAP. [i]DMSO/$NaBH_4$. [j]DMF/$NaBH_4$. [k]MeOH/NaOH/$NaBH_4$. [l]At 80 K, Na/THF. [m]DMF/THF/$NaBH_4$. [n]DMF/$NaBH_4$. [o]DMA/LiCl, bulk electrolysis. [p]DMA/$NaBH_4$. [q]DMSO/TBAP bulk electrolysis. [r]DMSO/$NaBH_4$.

https://doi.org/10.1021/acs.inorgchem.2c03456
Inorg. Chem. 2022, 61, 20177−20199

Indeed, it is well-known that the bulky PPh_3 axial ligand will not form a $PcFe^{II}(PPh_3)_2$ complex because of its large cone angle.[1] It is also well-documented that O-donor ligands coordinate to $PcFe^{II}$ only in the presence of CO gas, to form PcFeL(CO) compounds.[60−69] However, Lever's, Dzilinski's, and our EPR data clearly show that, once reduced, the $[PcFeL]^-$ and $[PcFeX]^{2-}$ complexes have high affinities for O-donor ligands and PPh_3 (Table 4). Indeed, DMF, DMA, MeO^-, and THF adducts have different EPR parameters (Table 4 and Figures S30−S33). One instructive EPR spectrum is shown in Figure 11

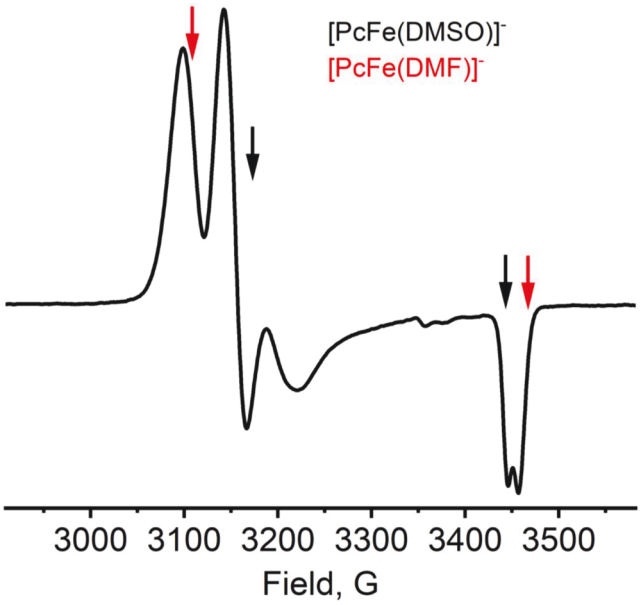

Figure 11. 77 K EPR spectrum of reduced iron phthalocyanine in a mixture of DMF and DMSO.

for the $[PcFeL]^-$ complexes (L = DMF or DMSO) which is clearly indicative of the presence of both DMF and DMSO adducts in solution. A similar result was observed for the DMA/THF mixture (Figure S30). Thus, in agreement with Lever and Wilshire, the EPR spectra of the $[PcFeL]^-$ and $[PcFeX]^{2-}$ complexes can be reasonably assigned as iron(I) d^7s = 1/2 systems of general formula $[Pc(2-)Fe^{I}L]^-$ and $[Pc(2-)Fe^{I}X]^{2-}$, which apparently contradicts the UV−vis and MCD data.

The ^{1}H NMR spectra of $[PcFe]^-$, $[PcFeL]^-$, and $[PcFeX]^{2-}$ complexes in THF-d_8, DMSO-d_6, DMSO-d_6/PPh_3, and DMF-d_7/KNCS are shown in Figures S1−S6. They consist of one (DMSO-d_6) or two (all other studied systems) broad signals observed between 15 and 17 ppm. The variable-temperature ^{1}H NMR spectra of $[PcFe(SCN)]^-$ in DMF-d_7 are shown in Figure 12. Upon reduction of the temperature, two initial broad signals observed at 15.07 and 16.13 ppm coalesce into a single peak around 240 K. The linear dependency between the chemical shifts for the phthalocyanine α- and β-protons and $1/T$ (Figure 12) suggests that the magnetic behavior of $[PcFe(NCS)]^{2-}$ (and highly likely all other complexes) follows Curie's law between 240 and 300 K. The solution magnetic moments for $[PcFe(DMSO)]^-$ in DMSO-d_6 and $[PcFe(NCS)]^{2-}$ in DMF-d_7 were measured using Evans method and were estimated to be 2.50 and 1.95 μ_B, respectively, which are indicative of an s = 1/2 spin system present in solution at room temperature. These values are comparable with the 2.12 μ_B magnetic moment for $Li^+[PcFe]^-$ reported by Taube in 1974.[4] However, they are significantly higher than the 1.69−1.74 μ_B values reported by Konarev and coauthors for similar compounds in the solid state.[85−88]

The Mössbauer spectrum of the solid $[PcFe]^-$ complex is complicated by its high sensitivity toward moisture and oxygen as well as a high affinity toward axial ligand coordination. Indeed, even when solid samples of the purple $[PcFe]^-$ complex were transferred to the Mössbauer sample holder inside a drybox, the recorded spectrum consisted of three doublets (Figure 13, left). The main doublet parameters belong to the $[PcFe]^-$ and are in excellent agreement with those reported by Taube in 1974[4] (Table 5). The other two minor doublets belong to the PcFe[116,117] and μ-oxo(1) $(PcFe)_2O$[118] complexes formed upon the oxidation of $[PcFe]^-$ by molecular oxygen diffused into the Mössbauer sample holder during the rapid transfer of the sample between the drybox and the Mössbauer instrument. Indeed, once the sample was purposefully exposed to air, the doublet associated with the $[PcFe]^-$ disappeared, while doublets associated with the μ-oxo(**1**) $(PcFe)_2O$ and PcFe complexes remained in the spectrum (Figure 13, right). As mentioned above, our Mössbauer data correlate well with those reported by Taube[4] but are in disagreement with the spectra obtained by Dzilinski and coauthors[94] (Table 5). Based on an experimental protocol Dzilinski and coauthors used for the sample preparation (room-temperature evaporation of the THF solution of the sample) and the high affinity of $[PcFe]^-$ toward

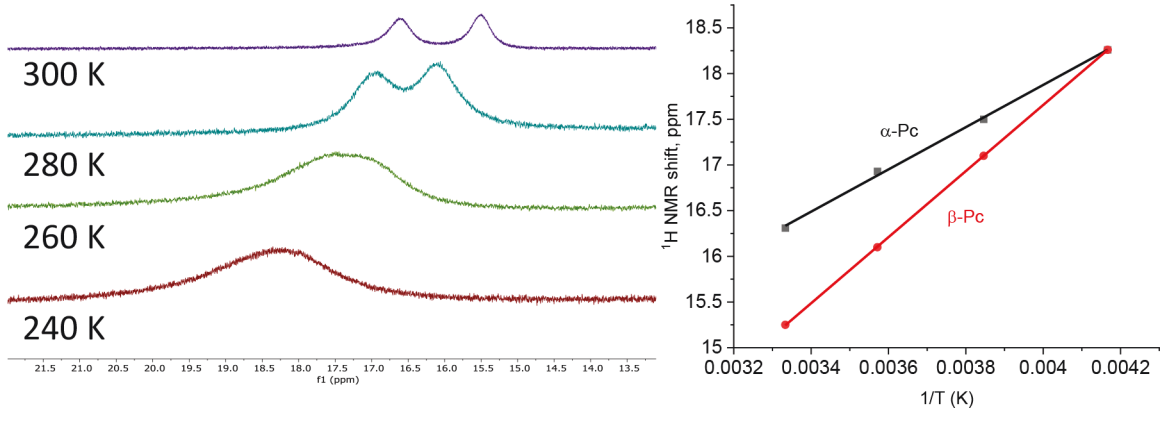

Figure 12. Variable-temperature partial ^{1}H NMR spectra of $[PcFe(NCS)]^{2-}$ in DMF-d_7 (left) and $1/T$ dependency of the chemical shifts (right).

https://doi.org/10.1021/acs.inorgchem.2c03456
Inorg. Chem. 2022, 61, 20177−20199

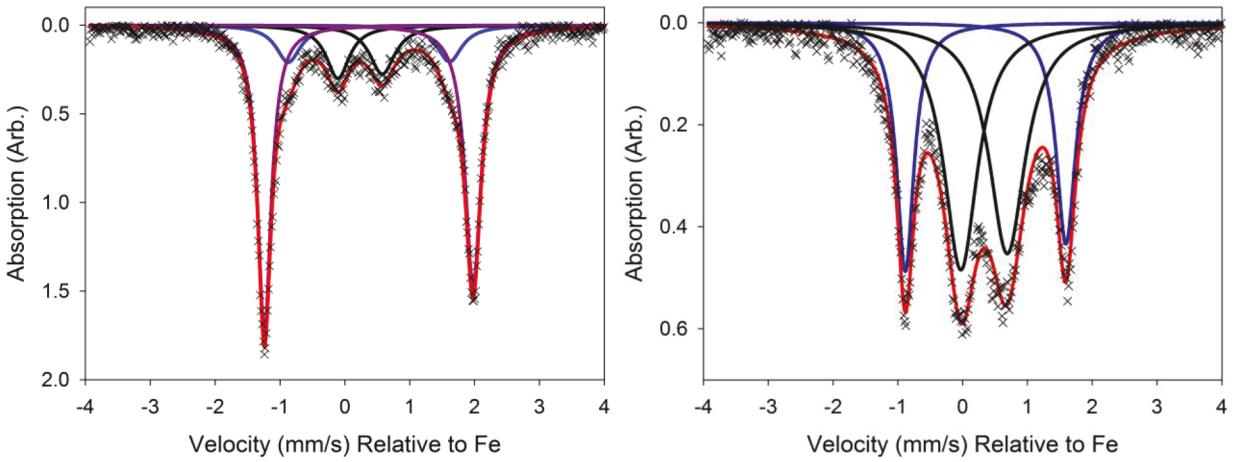

Figure 13. Solid-state room-temperature Mössbauer spectra of $[K(DME)_4][PcFe]$ (**1**) before (left) and after (right) exposure to air.

Table 5. Experimental and DFT-Predicted Mössbauer Parameters for PcFe-Based Systems

compound	method	temp	δ^a(mm/s)	ΔE(mm/s)	area (%)	ref[b]
$[PcFe]^-$	exptl	RT	0.37	3.22	64	tw
			0.35	2.48	17	tw
			0.23	0.69	19	tw
air exposed $[PcFe]^-$	exptl	RT	0.35	2.48	35	tw
			0.33	0.72	65	tw
$[PcFe]^-$	exptl	RT	0.35	3.24		4
$[PcFe]^-$	revTPSS/DMF		0.35	2.99		tw
$[PcFe]^-$	TPSSh/DMF		0.40	2.99		tw
$[PcFe(THF)]^-$	exptl	RT	0.38	2.80		94
$[PcFe(THF)]^-$	revTPSS/DMF		0.36	2.56		tw
$[PcFe(THF)]^-$	TPSSh/DMF		0.41	2.58		tw
PcFe		300 K	0.38	2.57		116
PcFe		293 K	0.40	2.62		117
$(PcFe)_2O$ (**1**)		295 K	0.25	0.42		118
$(FePc)_2O$ (**2**)		295 K	0.18	1.05		119

[a]Relative to natural Fe foil at 293 K. [b]tw = this work.

the axial ligand coordination as well as the DFT calculations presented below, we speculate that the Dzilinski's Mössbauer spectrum is that of the $[PcFe(THF)]^-$ complex. In both cases, the quadrupole splitting is larger than in the parent PcFe (which has a small dependency on the solid-state phase of this compound). In the simplistic point-charge model, Mössbauer quadrupole splitting can be calculated as sums of valence and lattice contributions according to eqs 4 and 5, respectively.[120,121]

$$q_{val} = (4/7)(1 - R)\langle r^{-3}\rangle_{3d}\{n(d_{xy}) + n(d_{x^2-y^2}) - n(d_{z^2}) - (1/2)[n(d_{xz}) + n(d_{yz})]\} + (4/5)(1 - R)\langle r^{-3}\rangle_{4p}\{(1/2)[n(p_x) + n(p_y)] - n(p_z)\} = k_{3d}\{n(d_{xy}) + n(d_{x^2-y^2}) - n(d_{z^2}) - (1/2)[n(d_{xz}) + n(d_{yz})]\} + k_{4p}\{(1/2)[n(p_x) + n(p_y)] - n(p_z)\} = k_{3d}\Delta n_{3d} + k_{4p}\Delta n_{4p} \quad (4)$$

$$q_{lat} = (1 - \gamma_\infty)\sum_{i=1}^{n}(q_i/r_i^3)(3\cos^2 q_i - 1) \quad (5)$$

where $\langle r^{-3}\rangle_{3d}$ and $\langle r^{-3}\rangle_{4p}$ are the expectation values of $1/r^3$ taken over the appropriate 3d and 4p radial functions at the iron atom, respectively. The terms $(1 - R)$ and $(1 - \gamma_\infty)$ are constants, and n is an effective population of the atomic orbitals designated by parentheses.

Assuming a $(d_{xy})^2(d_{xz,yz})^3(d_{z^2})^1$ electronic configuration in the parent $Pc(2-)Fe^{II}$ complex, addition of the extra electron to the d_π orbitals during the reduction process should increase the value of the q_{val} contribution and, thus, increase the quadrupole splitting in $[PcFe]^-$, in agreement with the experimental data. On the other hand, simultaneous reduction and axial coordination of the additional ligand along the z-axis should result in competing q_{val} and q_{lat}, leading to a smaller quadrupole splitting in $[PcFe(THF)]^-$ compared to $[PcFe]^-$. Thus, at first glance, again, the increase of the quadrupole splitting in single-electron-reduced $[PcFe(THF)]^-$ and $[PcFe]^-$ complexes compared to the parent PcFe seems to be indicative of the reduction of Fe^{II} to Fe^{I}. We will show below, however, that there is an alternative path that allows an increase in the electron density at the iron d_π orbitals without iron center reduction, which results in a similar increase of the quadrupole splitting in these compounds.

DFT and TDDFT Calculations. In order to resolve the dilemma regarding the reduction site in the $[PcFe]^-$, $[PcFeL]^-$, and $[PcFeX]^{2-}$ complexes, we have conducted an extensive array of DFT calculations on the $[PcFe]^-$, $[PcFeL]^-$, and $[PcFeX]^{2-}$ complexes, as well as the $[PcFeL_2]^-$ and $[PcFeX_2]^{3-}$

https://doi.org/10.1021/acs.inorgchem.2c03456
Inorg. Chem. 2022, 61, 20177−20199

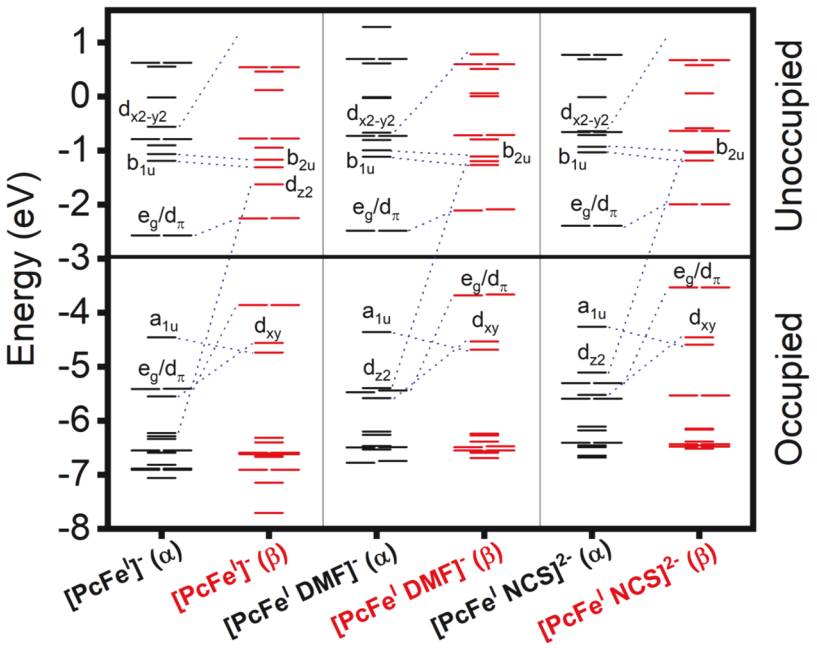

Figure 14. DFT-predicted (TPSSh/DMF) energy diagram for $[PcFe]^-$, $[PcFe(DMF)]^-$, and $[PcFe(NCS)]^{2-}$ complexes.

complexes. As we have shown previously,[57,59,98] the phthalocyanine-centered $1e_g^*$ MOs are always LUMO and LUMO + 1 in the initial neutral $PcFe^{II}L_2$ and $[PcFe^{II}X_2]^{2-}$ complexes. These orbitals are ∼1.5 eV more stable than the iron-centered unoccupied d_{z^2} orbital. In agreement with this electronic structure description, all hexacoordinated reduced $[PcFeL_2]^-$ and $[PcFeX_2]^{3-}$ complexes were predicted to have their spin density delocalized over the phthalocyanine ligand and, thus, should be described as $[Pc(3-)Fe^{II}L_2]^-$ and $[Pc(3-)Fe^{II}X_2]^{3-}$ compounds that retain low-spin iron(II) centers. However, from simple ligand field theory considerations,[122,123] one might expect that, upon losing one of the axial ligands (i.e., during the $[PcFeL_2]^- \rightarrow [PcFeL]^- + L$ process), the energy of the d_{z^2} orbital should reduce significantly. Such energy stabilization will place this orbital close to the iron-centered d_π and phthalocyanine-centered $1e_g^*$ MOs. In agreement with this hypothesis, the DFT-predicted electronic structures of the tetra- and pentacoordinate $[PcFe]^-$, $[PcFeL]^-$, and $[PcFeX]^{2-}$ compounds are very different from those in the hexacoordinate species. Indeed, in all cases, the lowest energy for tetra- and pentacoordinate complexes was achieved as the result of the antiferromagnetically coupled phthalocyanine anion radical $(1e_g^*)^1$ doublet and the iron(II) triplet state of the $(d_{xy})^2(d_{xz,yz})^3(d_{z^2})^1$ electron configurations.

The orbital energy diagram for selected single-electron-reduced compounds is presented in Figure 14, selected orbital images are shown in Figure 15 and Figures S32−S49, and their compositions are listed in Table 6 and Table S3. The representative examples for the total spin densities are shown in Figure 16 and are clearly supportive of the antiferromagnetic coupling between the reduced phthalocyanine ring and the iron(II) triplet. The presence of nearly two unpaired electrons at the iron center and nearly one unpaired electron at the phthalocyanine ring is evident from the Mulliken spin density population analysis shown in Table 7 and for select compounds using a large array of the exchange−correlation functionals in Table S2. The formation of the triplet iron(II) centers in tetra- and pentacoordinate $[PcFe]^-$, $[PcFeL]^-$, and $[PcFeX]^{2-}$

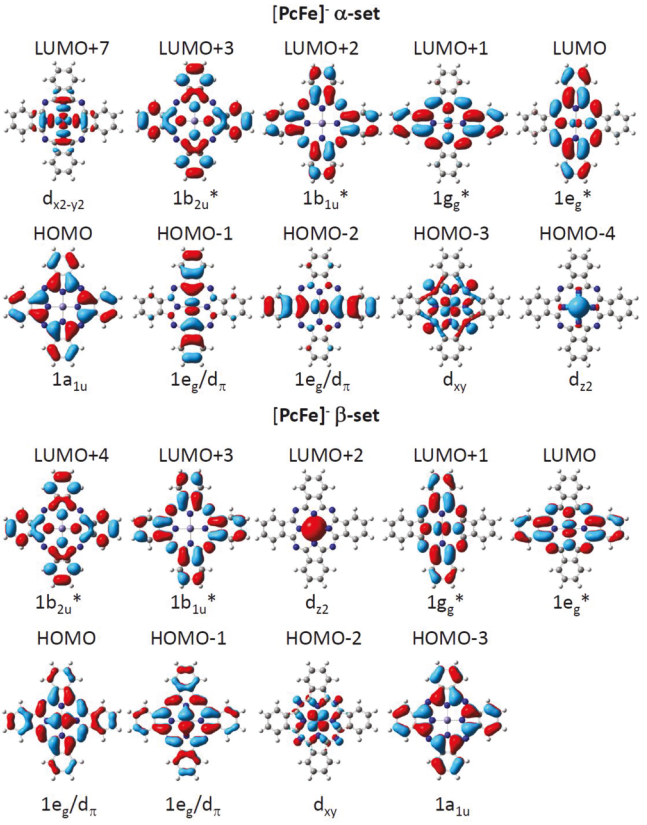

Figure 15. DFT-predicted (TPSSh/DMF) frontier MOs for $[PcFe]^-$. See Figures S32−S49 for MO images of all other compounds.

complexes is expected because of the decrease in the energy of the iron-centered d_{z^2} orbital upon dissociation of the axial ligand(s). Such a decrease of the energy leads to the situation when the electronic structure of the iron(II) center starts to resemble that of the square-planar $PcFe^{II}$ complex, which is known to have a $(d_{xy})^2(d_{xz,yz})^3(d_{z^2})^1$ triplet electronic configuration at the iron(II) center, although the $(d_{xy})^2(d_{z^2})^2(d_{xz,yz})^2$

https://doi.org/10.1021/acs.inorgchem.2c03456
Inorg. Chem. 2022, 61, 20177−20199

Table 6. DFT-Predicted Molecular Orbital Percent Contribution Distribution for $[PcFe]^{-}$[a]

$[PcFe]^{-}$ α-set				$[PcFe]^{-}$ β-set			
MO	E (eV)	% Fe	% Pc	MO	E (eV)	% Fe	% Pc
158	0.628	0.32	99.68	157	0.545	0.69	99.31
157	0.628	0.32	99.68	156	0.545	0.68	99.32
156	0.554	0	100	155	0.464	0	100
155	−0.014	92.26	7.74	154	0.121	93.09	6.91
154	−0.558	43.01	56.99	153	−0.777	3.07	96.93
153	−0.787	0.73	99.27	152	−0.777	3.08	96.92
152	−0.787	0.73	99.27	151	−0.944	1.93	98.07
151	−0.903	2.79	97.21	150	−1.17	0	100
150	−1.065	0	100	149	−1.307	0	100
149	−1.187	0	100	148	−1.622	94.06	5.94
148	−2.568	3.66	96.34	147	−2.251	31.87	68.13
147	**−2.568**	**3.66**	**96.34**	**146**	**−2.253**	**31.72**	**68.28**
146	**−4.456**	**0**	**100**	**145**	**−3.858**	**39.46**	**60.54**
145	−5.408	55.75	44.25	144	−3.86	39.66	60.34
144	−5.41	55.68	44.32	143	−4.559	64.46	35.54
143	−5.548	57.84	42.16	142	−4.738	0	100
142	−6.228	94.71	5.29	141	−6.315	0	100
141	−6.286	0	100	140	−6.4	0.45	99.55
140	−6.338	0.48	99.52	139	−6.593	2.17	97.83
139	−6.548	0.06	99.94	138	−6.593	2.1	97.9
138	−6.549	0.06	99.94	137	−6.601	1.5	98.5
137	−6.586	0	100	136	−6.617	4.49	95.51
136	−6.589	2.04	97.96	135	−6.617	4.45	95.55
135	−6.813	14.03	85.97	134	−6.635	0	100
134	−6.887	0.2	99.8	133	−6.666	3.92	96.08
133	−6.887	0.2	99.8	132	−6.904	0.18	99.82
132	−6.906	35.63	64.37	131	−6.904	0.18	99.82
131	−6.907	35.7	64.3	130	−7.147	0	100
130	−7.058	0	100	129	−7.706	0.24	99.76

[a]The HOMO and LUMO are formatted in bold.

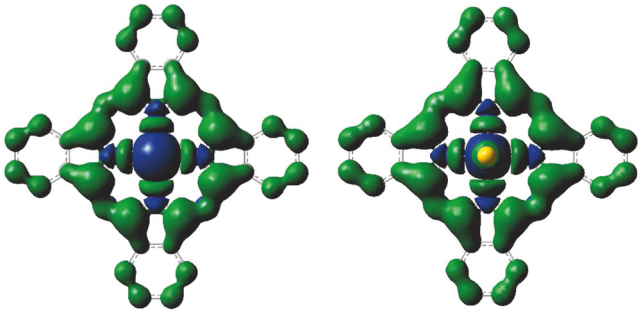

Figure 16. DFT-predicted (TPSSh/DMF) total spin densities of $[PcFe]^{-}$ (left) and $[PcFe(NCS)]^{2-}$ (right) anions showing antiferromagnetic interactions between Pc(3−) and Fe^{II} (s = 1).

triplet configuration is also close in energy.[117,124−127] Thus, the single-electron-reduced iron(II) phthalocyanines should be formulated as $[Pc(3-)Fe^{II}]^{-}$, $[Pc(3-)Fe^{II}L]^{-}$, and $[Pc(3-)Fe^{II}X]^{2-}$ species in which the ring-reduced phthalocyanine core is antiferromagnetically coupled with the iron(II) s = 1 center.

From the mechanistic single-electron determinant based point of view, the one-electron-reduction process for hexacoordinate $PcFeL_2$ and $[PcFeX_2]^{2-}$ complexes can be described in three steps (Figure 17). In the first step, the phthalocyanine-centered $1e_g$* MOs accept an electron to form $[Pc(3-)Fe^{II}L_2]^{-}$ or $[Pc(3-)Fe^{II}X_2]^{2-}$ species that carry low-spin iron(II) centers (Figure 17B). The axial ligand dissociation lowers the energy of the iron-centered d_{z^2} orbital (Figure 17C). Finally, the electron transfer from d_π orbitals to the d_{z^2} orbital transforms the low-spin iron(II) ion into the triplet state and provides the pathway for the antiferromagnetic coupling between iron-centered $(d_{xz,yz})^3$ and phthalocyanine-centered $(1e_g^*)^1$ orbitals (Figure 17D). From a mechanistic point of view, the tetracoordinate PcFe complex already has a triplet $(d_{xy})^2(d_{xz,yz})^3(d_{z^2})^1$ electronic configuration (Figure 17E). Thus, the addition of a single electron directly to the phthalocyanine-centered $1e_g$* MOs should lead to the formation of the $[Pc(3-)Fe^{II}]^{-}$ complex in which iron-centered $(d_{xz,yz})^3$ electrons are antiferromagnetically coupled to the phthalocyanine-centered $(1e_g^*)^1$ orbitals (Figure 17D). It is obvious that the above-described single-electron approximation can only be used for illustrative purposes as the iron-centered d_π MOs of e_g (in traditional for phthalocyanines D_{4h} point group notation) or e (in the C_{4v} point group) symmetry will interact strongly with the phthalocyanine-centered $1e_g$* MOs (Table 3). As a result, the occupied MOs of the α-set will only slightly be dominated by the contribution from the iron d_π atomic orbitals, while the β-set MOs will be dominated by the phthalocyanine-centered MOs, resulting in an overall $(d_{xz,yz})^3(1e_g^*)^1$ electronic configuration in the $[PcFe]^{-}$, $[PcFeL]^{-}$, and $[PcFeX]^{2-}$ complexes. Independent of the approach used (molecular orbital analysis or NBO analysis discussed below), our DFT calculations suggest that the electron gained by the iron(II) phthalocyanine upon the reduction process is localized at the phthalocyanine core. Thus, the DFT-predicted electronic structure of these compounds can be viewed as $[Pc(3-)Fe^{II}]^{-}$, $[Pc(3-)Fe^{II}L]^{-}$, and $[Pc(3-)Fe^{II}X]^{2-}$ with Fe^{II} triplet centers.

Table 7. DFT-Predicted Mulliken Total Spin Densities at the Iron Center in $[PcFe]^{-}$, $[PcFeL]^{-}$, and $[PcFeX]^{2-}$ Complexes

compound	TPSSh (gas)	TPSSh (DMF)	revTPSS (DMF)
$[PcFe]^{-}$	1.94	1.97	1.74
$[PcFePy]^{-}$	1.94	1.98	1.77
$[PcFeIm]^{-}$	1.97	2.02	1.81
$[PcFe(NCS)]^{2-}$	2.15	2.07	1.84
$[PcFe(PPh_3)]^{-}$	1.90	1.93	1.56
$[PcFe(OMe)]^{2-}$	2.38	2.32	2.09
$[PcFe(THF)]^{-}$	1.99	2.01	1.81
$[PcFe(DMF)]^{-}$	2.00	2.05	1.83
$[PcFe(DMSO)]^{-}$	1.84	1.87	1.63

The natural bond orbital (NBO) analysis reveals approximately a three-electron occupancy of the iron d_{xzyz} orbitals and a one-electron-occupied d_{z^2} orbital in the reduced compounds. For instance, in the case of $[PcFe]^{-}$ and $[PcFe(NCS)]^{2-}$, the NBO analysis predicts $(d_{xy})^{1.87}(d_{xz,yz})^{3.02}(d_{z^2})^{1.02}$ and $(d_{xy})^{1.97}(d_{xz,yz})^{2.82}(d_{z^2})^{1.16}$ electronic configurations, respectively. The typical electronic configuration for the parent $PcFe^{II}L_2$ and $[PcFe^{II}X_2]^{2-}$ complexes evaluated by NBO analysis is $(d_{xy})^{1.97-1.98}(d_{xz,yz})^{3.50-3.64}(d_{z^2})^{0.72-0.78}$.[59] Thus, it is clear the NBO analysis predicts that, upon single-electron reduction, the population of the d_{z^2} orbital increases while the population of the d_π orbitals decreases, in agreement with the DFT-predicted electronic structures and total spin densities of these compounds. Next, we need to explore how such an unusual electronic configuration $((d_{xy})^2(d_{xz,yz})^3(d_{z^2})^1(1e_g^*)^1)$ of single-electron-reduced iron phthalocyanines will correlate with the EPR, UV−vis, MCD, and Mössbauer spectra observed for these compounds.

https://doi.org/10.1021/acs.inorgchem.2c03456
Inorg. Chem. 2022, 61, 20177−20199

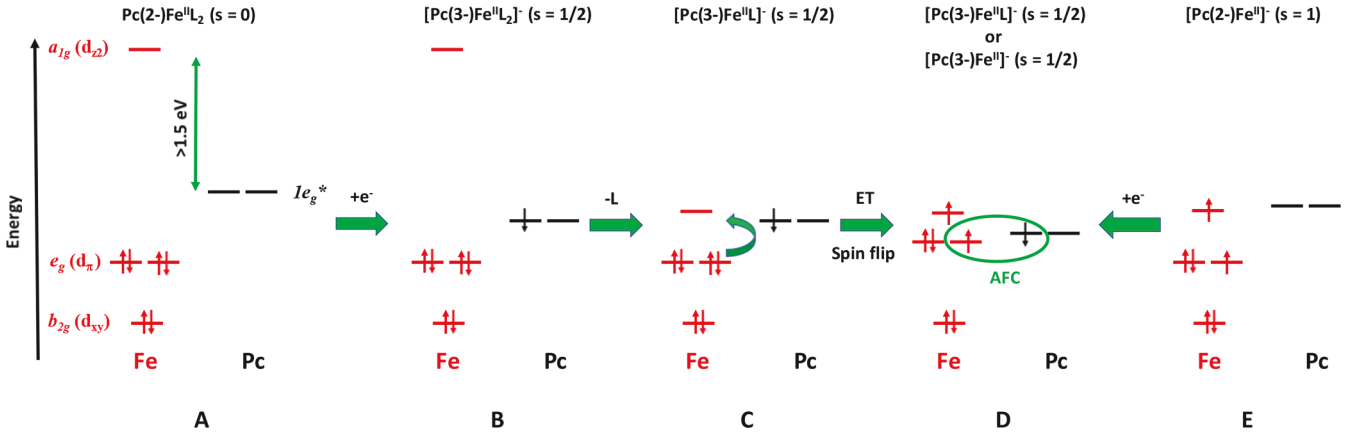

Figure 17. Proposed mechanism of the formation of the $[Pc(3-)Fe^{II}]^-$ and $[Pc(3-)Fe^{II}L]^-$ complexes from $Pc(2-)Fe^{II}L_2$ and $Pc(2-)Fe^{II}$ compounds upon single-electron reduction.

The DFT-predicted EPR spectra for the tetra- and pentacoordinate $[PcFe]^-$, $[PcFeL]^-$, and $[PcFeX]^{2-}$ complexes calculated using several exchange−correlation functionals are listed in Table 4. As is evident from the *g*-values listed in Table 4, the DFT-predicted EPR spectra are nearly axial and overall the spectra correlate very well with the experimental data. The DFT-predicted values of superhyperfine splitting for the $[Pc(3-)Fe^{II}L]^-$ complexes (L = Py, Im, and PPh_3) again correlate well with the experimental data. The overall EPR spectra predicted by DFT resemble the axial $s = 1/2$ spectra rather than those expected for a phthalocyanine anion radical (an isotropic signal with a *g*-value close to 2.0).[79,99−101] They clearly indicate significant antiferromagnetic coupling between $(d_{xz,yz})^3$ and $(1e_g^*)^1$ configurations, which results in the EPR spectra that resemble overall iron-centered $s = 1/2$ systems (Figure 17). The strong antiferromagnetic coupling to the iron triplet state center leading to EPR spectra close to those observed for odd-electron systems has been reported in the literature. In particular, $(corrole)^{\bullet+}Fe^{IV}$ complexes and antiferromagnetically coupled metalloenzymes in a compound-I-like state (in which a porphyrin cation radical is antiferromagnetically coupled to the iron oxoferryl triplet state) give rise to EPR spectra close to those of iron(III) low-spin systems.[128−131] Similarly, ferromagnetically coupled $Fe^{IV}{=}O$ ($s = 1$) and porphyrin cation radical ($s = 1/2$) compound I analogues have EPR spectra that resemble, to a large extent, iron(III) intermediate-spin ($s = 3/2$) systems.[132−135] Overall, the DFT-predicted EPR spectra using several exchange−correlation functionals correlate well with the experimental data, with the TPSS functional providing the best agreement between theory and experiment. The DFT-predicted EPR spectra are indicative of the axial symmetry and overall $s = 1/2$ ground state in $[PcFe]^-$, $[PcFeL]^-$, and $[PcFeX]^{2-}$ complexes that formed as a result of antiferromagnetic coupling between metal-centered $(d_{xy})^2(d_{xz,yz})^3(d_{z^2})^1$ and phthalocyanine-centered $(1e_g^*)^1$ electronic configurations.

The DFT-predicted Mössbauer isomer shifts and quadrupole splittings for the compounds of interest are listed in Table 5 along with the experimental data. The DFT-predicted values are in reasonable agreement with the experimental data, clearly showing the decrease of the quadrupole splitting upon axial coordination of the THF ligand compared to the square-planar species. Although the calculated quadrupole splittings are systematically underestimated, their errors (∼10%) are within the expected range for modern DFT methods.[59,136] Again, our DFT calculations show that, in agreement with the experimental data, the $(d_{xy})^2(d_{xz,yz})^3(d_{z^2})^1(1e_g^*)^1$ electronic configuration leads to a larger quadrupole splitting in $[PcFe]^-$ and $[PcFe(THF)]^-$ complexes compared to the parent PcFe.

The TDDFT calculations were used to explain the overall shape and the nature of the experimentally observed transitions in the UV−vis and MCD spectra of the $[PcFe]^-$, $[PcFeL]^-$, and $[PcFeX]^{2-}$ complexes. We used $[PcFe]^-$, $[PcFe(DMF)]^-$, and $[PcFe(NCS)]^{2-}$ complexes as the representative examples of tetracoordinate and pentacoordinate mono- and dianions, respectively. The TDDFT-predicted spectra are compared to experimental data in Figure 18, while the expansion coefficients for the selected transitions are listed in Table 8. In general, the TDDFT calculations were able to reproduce the general shape of the observed spectra. In particular, the TDDFT calculations predicted that the UV−vis spectra in $[PcFe]^-$, $[PcFeL]^-$, and $[PcFeX]^{2-}$ complexes should be dominated by strong transitions around 500 nm, which are responsible for the purple/red color of these compounds. According to the TDDFT calculations, the experimentally observed band at ∼800−830 nm is dominated by the $1a_{1u}(\alpha) \rightarrow 1e_g^*$ single-electron transition and thus can be assigned as the Q-band. A similar Q-band, which is associated with two MCD opposite sign *B*-terms, was observed at ∼930 nm in $[Pc(3-)M^{II}]^-$ complexes (M = Zn or Mg) by Stillman and co-workers.[99−101] Again, the calculated overall split between Q_x and Q_y components is rather small (1−40 cm^{-1}) and correlates well with the experimental data. The TDDFT calculations predict three pairs of degenerate (or nearly degenerate) intense transitions in the 400−620 nm spectral envelope of $[PcFe]^-$ (Figure 18). The first band was predicted at 567 nm and is dominated by the $1a_{1u}(\beta) \rightarrow 1e_g^*$ single-electron excitations that are complemented by the $1e_g(Pc)/d_\pi(\beta) \rightarrow 1b_{2u}^*(Pc)$ contributions (Table 8). The second pair of transitions was predicted at 515 nm and has the highest intensity in this spectral envelope. This band is dominated by $1e_g(Pc)/d_\pi(\beta) \rightarrow 1b_{2u}^*(Pc)$ single-electron excitations and resembles the $MLCT_2$ band observed in the $Pc(2-)Fe^{II}L_2$ and $[Pc(2-)Fe^{II}X_2]^{2-}$ complexes.[98] The pair of degenerate transitions that are dominated by the $1e_g(Pc)/d_\pi(\beta) \rightarrow 1b_{1u}^*(Pc)$ single-electron transitions (band that resembles $MLCT_1$ transition in $Pc(2-)Fe^{II}L_2$ and $[Pc(2-)Fe^{II}X_2]^{2-}$ complexes)[98] was predicted to have zero intensity (Table 8). Finally, the third pair of degenerate transitions was predicted at 480 nm and has a significant MLCT character (Table 8). Addition of the fifth ligand at the axial position to the $[PcFe]^-$ complex leads to a substantial increase of the intensity of the

https://doi.org/10.1021/acs.inorgchem.2c03456
Inorg. Chem. 2022, 61, 20177−20199

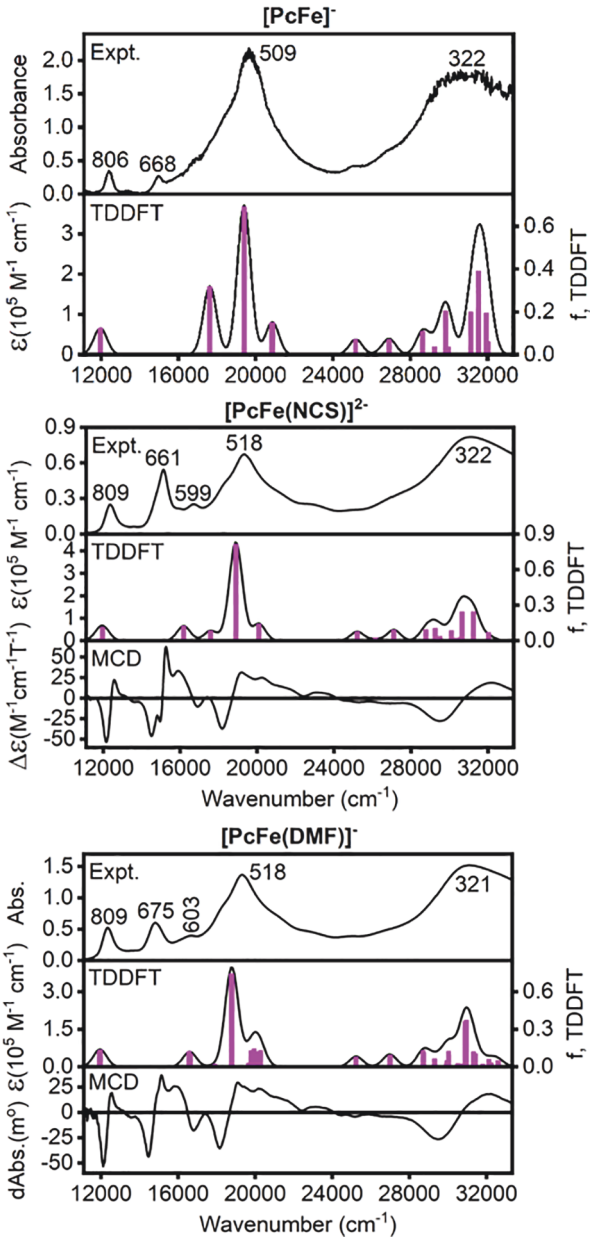

Figure 18. Comparison between experimental and TDDFT-predicted UV−vis spectra of $[PcFe]^-$, $[PcFe(DMF)]^-$, and $[PcFe(NCS)]^{2-}$ compounds.

band that has significant $MLCT_1$ character. This band was predicted at 602 nm in $[PcFe(DMF)]^-$ and 618 nm in $[PcFe(NCS)]^{2-}$ complexes. The lower energy of this band compared to that predicted for $[PcFe]^-$ reflects the destabilization of the occupied $1e_g/d_\pi$ orbital upon axial ligand coordination. Thus, one might speculate that the experimentally observed in the ∼650−690 nm range MCD pseudo *A*-term in $[PcFeL]^-$ and $[PcFeX]^{2-}$ complexes has substantial $MLCT_1$ character. The presence of this band in the UV−vis spectrum of tetracoordinate $[PcFe]^-$ reflects either the presence of a small amount of water or THF in solution (Figure 8) or the ability of the symmetry forbidden transition to gain intensity through a vibronic mechanism (which is, however, unlikely to give the observed intensity of this band). The TDDFT-predicted $MLCT_1$−$MLCT_2$ energy gaps are 1690, 1400, and 1280 cm^{-1} for $[PcFe]^-$, $[PcFe(NCS)]^{2-}$, and $[PcFe(DMF)]^-$ complexes, which correlate well with the $MLCT_1$−$MLCT_2$ energy gap observed in the parent $Pc(2-)Fe^{II}L_2$ and $[Pc(2-)Fe^{II}X_2]^{2-}$ complexes and indirectly measures the $1b_{1u}$*−$1b_{2u}$* energy difference (Figure 1). For the $[Pc(3-)M]^-$ and $[Pc(3-)ML]^-$ complexes (M = Mg or Zn), Stillman and co-workers have reasonably assumed that the energy difference between the most intense *B*-terms of negative and positive amplitudes in the ∼500−600 nm region can be used as a direct experimental measure of the $1b_{1u}$*−$1b_{2u}$* energy gap.[99−101] Our TDDFT calculations are in reasonable agreement with the Stillman predictions. However, if one would assume that the experimentally observed MCD pseudo *A*-term in the ∼650−690 nm area belongs to the $MLCT_1$ band and another pseudo *A*-term observed around 515 nm belongs to the $MLCT_2$ band, then the $1b_{1u}$*−$1b_{2u}$* energy gap should be significantly larger than that predicted by TDDFT calculations. One important fact we would like to mention is that the $MLCT_1$ and $MLCT_2$ bands in $Pc(2-)Fe^{II}L_2$ and $[Pc(2-)Fe^{II}X_2]^{2-}$ complexes are heavily dominated by the $1e_g/d_\pi \rightarrow 1b_{1u}$* and $1e_g/d_\pi \rightarrow 1b_{2u}$* single-electron contributions,[98] while much stronger configurational interactions were predicted for the same transitions in the $[PcFe]^-$, $[PcFe(DMF)]^-$, and $[PcFe(NCS)]^{2-}$ complexes (Table 8).

Overall, our DFT and TDDFT calculations explain well the presence of the axial $s = 1/2$ EPR spectra as well as Pc(3−)-like UV−vis and MCD spectra in the $[PcFe]^-$, $[PcFeL]^-$, and $[PcFeX]^{2-}$ complexes, thus resolving the apparent locus-of-reduction controversy for these compounds discussed for 50 years. The DFT- and TDDFT-predicted EPR, Mössbauer, and UV−vis spectra of the $[PcFe]^-$, $[PcFeL]^-$, and $[PcFeX]^{2-}$ complexes are in good agreement with the experimental data and are indicative of a single-electron-reduced phthalocyanine ligand that is antiferromagnetically coupled with an intermediate-spin ($s = 1$) iron(II) center.

CONCLUSIONS

The purple/red $[PcFe]^-$, $[PcFeL]^-$ (L = Py, Im, PPh_3, THF, DMF, DMA, and DMSO), and $[PcFeX]^{2-}$ (X = NCS^- or MeO^-) anions were prepared *in situ* or isolated by the reduction of iron(II) phthalocyanine ($Pc(2-)Fe^{II}$) or its bisaxially coordinated $PcFeL_2$ or $[PcFeX_2]^{2-}$ complexes under chemical or spectroelectrochemical reduction conditions. $[K(DME)_4]$-[PcFe] was characterized by X-ray crystallography and was found to consist of the square-planar $[PcFe]^-$ anion with a flat phthalocyanine macrocycle. Room- and variable-temperature ^1H NMR spectra as well as solution magnetic moments of the reduced species are consistent with the paramagnetic nature of all complexes and the presence of a single unpaired electron. A solid-state Mössbauer spectrum of $[K(DME)_4][PcFe]$ is consistent with the early report by Taube.[4] Solution EPR spectra of $[PcFeL]^-$ and $[PcFeX]^{2-}$ complexes have axial symmetry and correlate well with spectra reported by Lever in 1978.[71] The UV−vis and MCD spectra of pentacoordinate $[PcFeL]^-$ and $[PcFeX]^{2-}$ anions consist of the characteristic bands around 810, 690, and 515 nm, which have only slight axial ligand dependency and are essentially independent of temperature. A ∼660−690 nm band exhibits significantly lower intensity in the square-planar $[PcFe]^-$ complex. Thus, this band can be used as a diagnostic transition to differentiate between tetra- and pentacoordinate species. The UV−vis and MCD spectra of $[PcFeL]^-$ and $[PcFeX]^{2-}$ complexes are in stark contrast to the crystallographically characterized reference $[Pc(2-)Co^I]^-$ anion, which is EPR silent, has a regular

https://doi.org/10.1021/acs.inorgchem.2c03456
Inorg. Chem. 2022, 61, 20177−20199

Table 8. Major TDDFT-Predicted Excited State Contributions for $[PcFe]^-$, $[PcFe(NCS)]^{2-}$, $[PcFe(DMF)]^-$ Complexes Using the TPSSh Exchange−Correlation Functional in DMF

ES	λ (nm)	E (cm^{-1})	oscillator strength, f	% contribution
				$[PcFe]^-$
10, 11	836	11960	0.1229	H(α) → L/L + 1(α) (87%),H − 3(β) → L/L + 1(β) (9%)
12, 13	567	17630	0.3152	H − 3(β) → L/L + 1(β) (64%),H/H − 1(β) → L + 4(β) (18%),H/H − 1(β) → L + 3(β) (11%)
20, 21	515	19399	0.6889	H/H − 1(β) → L + 4(β) (73%),H/H − 1(β) → L + 3(β) (12%)
25, 26	479	20861	0.1498	H/H − 1(β) → L + 5(β) (95%)
38, 39	379	25183	0.0702	H − 5(α) → L/L + 1(α) (29%),H − 6(α) → L/L + 1(α) (18%),H(α) → L + 5/L + 6(α) (16%)
49, 50	371	26920	0.0704	H − 5(α) → L/L + 1(α) (43%),H − 6(α) → L/L + 1(α) (17%),H(α) → L + 5/L + 6(α) (15%)
55, 56	349	28655	0.1082	H − 10(α) → L/L + 1(α) (39%),H − 5(α) → L/L + 1(α) (18%)
62, 63	342	29261	0.0365	H − 3(β) → L + 6/L + 7(β) (52%),H − 10(α) → L/L + 1(α) (16%),H(α) → L + 5/L + 6(α) (12%), H − 9(α) → L/L + 1(α) (11%)
65, 66	335	29827	0.2033	H − 9(α) → L/L + 1(α) (72%),H − 3(β) → L + 6/L + 7(β) (12%)
70, 71	334	29985	0.0340	H − 4(β) → L/L + 1(β) (75%)
79, 80	321	31127	0.1936	H − 5(β) → L/L + 1(β) (45%),H − 1/H − 2(α) → L + 2(α) (31%),H − 6(α) → L/L + 1(α) (12%)
83, 84	317	31547	0.3851	H − 1/H − 2(α) → L + 2(α) (38%),H/H − 1(β) → L + 9(β) (15%),H − 5(β) → L/L + 1(β) (15%), H − 10(α) → L/L + 1(α) (12%)
86, 87	313	31934	0.1945	H − 1/H − 2(α) → L + 3(α) (63%),H − 8(β) → L/L + 1(β) (14%)
90, 91	312	32034	0.0587	H/H − 1(β) → L + 9(β) (19%),H − 1/H − 2(α) → L + 2(α) (18%),H − 8(β) → L/L + 1(β) (16%)
				$[PcFe(NCS)]^{2-}$
7, 8	851	11748	0.0170	H/H − 1(β) → L + 3(β) (54%),H(α) → L/L + 1(α) (21%),H/H − 1(β) → L + 7(β) (14%)
9, 10	835	11973	0.1114	H(α) → L/L + 1(α) (67%),H/H − 1(β) → L + 3(β) (16%)
12, 13	618	16186	0.1211	H/H − 1(β) → L + 2(β) (79%),H/H − 1(β) → L + 4(β) (16%)
15, 16	569	17583	0.0808	H/H − 1(β) → L + 4(β) (56%),H − 1(α) → L/L + 1(α) (17%),H − 3(β) → L/L + 1(β) (15%)
19, 20	529	18896	0.8117	H − 3(β) → L/L + 1(β) (50%),H/H − 1(β) → L + 4(β) (21%),H − 1(α) → L/L + 1(α) (14%)
24, 25	498	20092	0.1395	H − 5(α) → L + 1(α) (40%),H − 6(α) → L(α) (40%)
45, 46	397	25203	0.0748	H(α) → L + 5/L + 6(α) (30%),H − 7(α) → L/L + 1(α) (25%),H − 8(α) → L/L + 1(α) (12%)
53	382	26148	0.0238	H − 5(β) → L + 1(β) (49%),H − 4(β) → L(β) (47%)
60, 61	369	27107	0.0890	H − 8(α) → L/L + 1(α) (36%),H − 7(α) → L/L + 1(α) (34%),H − 7(β) → L/L + 1(β) (13%), H − 12(α) → L/L + 1(α) (10%)
66, 67	347	28777	0.0938	H − 3(β) → L + 5/L + 6(β) (22%),H − 12(α) → L/L + 1(α) (20%),H − 7(α) → L/L + 1(α) (13%)
70, 71	342	29263	0.1039	H − 3(β) → L + 5/L + 6(β) (36%),H − 12(α) → L/L + 1(α) (20%),H/H − 1(β) → L + 12(β) (10%)
72, 73	339	29499	0.0368	H/H − 1(β) → L + 12(β) (33%),H − 2/H − 3(α) → L + 7(α) (18%),H − 3(β) → L + 5/L + 6(β) (15%), H − 13(α) → L/L + 1(α) (11%)
78, 79	332	30101	0.0843	H − 11(α) → L/L + 1(α) (66%)
81, 82	330	30335	0.0212	H − 13(α) → L/L + 1(α) (60%)
84, 85	327	30573	0.0284	H/H − 1(β) → L + 9(β) (29%),H − 6(β) → L/L + 1(β) (27%),H − 12(α) → L/L + 1(α) (24%), H − 7(β) → L/L + 1(β) (11%)
86, 87	326	30646	0.2434	H − 6(β) → L/L + 1(β) (44%),H/H − 1(β) → L + 9(β) (39%)
93, 94	320	31246	0.2437	H − 7(β) → L/L + 1(β) (45%),H − 8(α) → L/L + 1(α) (12%),H/H − 1(β) → L + 9(β) (11%)
100	312	32035	0.0694	H − 2(α) → L + 2(α) (66%)
				$[PcFe(DMF)]^-$
9, 10	837	11951	0.1292	H(α) → L/L + 1(α) (89%)
11, 12	602	16610	0.1119	H/H − 1(β) → L + 2(β) (79%),H/H − 1(β) → L + 4(β) (17%)
14	558	17908	0.0205	H(β) → L + 4(β) (44%), H − 3(β) → L + 1(β) (42%), H − 1(β) → L + 2(β) (12%)
17, 18	532	18789	0.7372	H − 3(β) → L/L + 1(β) (45%), H/H − 1(β) → L + 4(β) (33%)
19	508	19668	0.0297	H − 1(α) → L + 1(α) (35%),H − 2(α) → L(α) (27%),H − 3(α) → L + 1(α) (11%)
20	505	19794	0.1289	H − 1(α) → L(α) (82%)
21	501	19950	0.1436	H − 1(α) → L + 1(α) (49%),H − 3(α) → L + 1(α) (19%),H − 2(α) → L(α) (11%)
22	499	20021	0.0328	H − 2(α) → L + 1(α) (53%),H − 3(α) → L(α) (18%)
23	496	20150	0.1200	H(β) → L + 5(β) (66%)
24	493	20266	0.0127	H(β) → L + 7(β) (32%),H − 3(α) → L + 1(α) (19%),H(β) → L + 5(β) (17%),H − 1(β) → L + 6(β) (15%)
25	493	20283	0.1299	H − 1(β) → L + 5(β) (83%)
40, 41	396	25241	0.0761	H − 5(α) → L/L + 1(α) (28%),H(α) → L + 5/L + 6(α) (24%),H − 6(α) → L/L + 1(α) (14%)
51	373	26778	0.0110	H − 1(β) → L + 8(β) (88%)
52, 53	370	26995	0.0845	H − 5(α) → L/L + 1(α) (36%),H − 6(α) → L/L + 1(α) (30%),H − 5(β) → L/L + 1(β) (10%), H − 11(α) → L/L + 1(α) (10%)
61, 62	348	28731	0.1197	H − 11(α) → L/L + 1(α) (30%), H − 5(α) → L/L + 1(α) (15%), H − 3(β) → L + 6/L + 7(β) (10%)
65, 66	341	29315	0.0605	H − 3(β) → L + 6/L + 7(β) (75%), H − 11(α) → L/L + 1(α) (17%)
70, 71	334	29940	0.0394	H − 12(α) → L/L + 1(α) (41%),H/H − 1(β) → L + 13(β) (20%),H − 2/H − 3(α) → L + 7(α) (12%), H − 10(α) → L/L + 1(α) (10%)
72	333	30035	0.0486	H − 10(α) → L + 1(α) (22%),H − 13(α) → L + 1(α) (17%),H − 14(α) → L(α) (16%), H − 8(α) → L + 1(α) (13%)

https://doi.org/10.1021/acs.inorgchem.2c03456
Inorg. Chem. 2022, 61, 20177−20199

Table 8. continued

ES	λ (nm)	E (cm^{-1})	oscillator strength, f	% contribution
				[PcFe(DMF)]$^-$
73	333	30039	0.1238	H − 10(α) → L(α) (51%),H − 11(α) → L(α) (11%)
74	333	30039	0.0958	H − 10(α) → L + 1(α) (45%)
79	328	30512	0.0257	H − 12(α) → L + 1(α) (26%), H − 4(β) → L(β) (17%),H − 1(β) → L + 13(β) (15%), H − 2(α) → L + 7(α) (13%),H − 11(β) → L + 1(β) (10%)
81	325	30738	0.0229	H − 7(α) → L + 1(α) (14%), H − 8(β) → L(β) (13%),H − 8(α) → L(α) (12%),H − 13(α) → L(α) (11%)
82, 83	323	30929	0.3671	H/H − 1(β) → L + 10(β) (47%),H − 5(β) → L/L + 1(β) (20%)
87	319	31329	0.1192	H(β) → L + 10(β) (32%),H − 5(β) → L(β) (32%),H − 6(α) → L(α) (10%)
89	318	31424	0.1042	H − 1(β) → L + 10(β) (33%),H − 5(β) → L + 1(β) (31%)
91	314	31807	0.0223	H − 1(α) → L + 2(α) (75%)
96	311	32131	0.0602	H − 2(α) → L + 2(α) (28%),H − 7(β) → L(β) (22%),H − 11(β) → L(β) (13%)
98	310	32254	0.0310	H − 3(α) → L + 2(α) (30%),H − 7(β) → L + 1(β) (28%),H − 11(β) → L + 1(β) (11%)
99	307	32594	0.0491	H − 2(α) → L + 2(α) (43%),H − 7(β) → L(β) (41%)
100	307	32626	0.0410	H − 1(α) → L + 3(α) (32%),H − 15(α) → L(α) (17%),H − 3(α) → L + 3(α) (10%)

diamagnetic ^{1}H NMR spectrum, and has an intense ($\varepsilon \sim 10^5$ M^{-1} cm^{-1}) Q-band at 699 nm, which correlates well with the strong MCD *A*-term. DFT and TDDFT calculations are suggestive of the iron(II) center in the $(d_{xy})^2(d_{xz,yz})^3(d_{z^2})^1$ (s = 1) electronic configuration that is antiferromagnetically coupled with the one-electron-reduced Pc(3−) ligand (i.e., $[Pc(3-)Fe^{II}]^-$, $[Pc(3-)Fe^{II}L]^-$, and $[Pc(3-)Fe^{II}X]^{2-}$). The calculated using several exchange−correlation functionals EPR, Mössbauer, and UV−vis spectra of the $[PcFe]^-$, $[PcFeL]^-$ and $[PcFeX]^{2-}$ complexes are in excellent agreement with the experimental data, thus resolving the apparent contradiction between the axial s = 1/2 EPR and Pc(3−)-like UV−vis spectra of these compounds.

EXPERIMENTAL SECTION

Materials. All solvents were purchased from commercial sources and purified with the use of standard procedures. Except for the reduced PcFe and PcCo in DME outlined below, all compounds were prepared as described previously.[45,61] For the chemical reduction of PcFe and PcCo, all procedures were carried out under a nitrogen atmosphere in an MBraun Labmaster 130 glovebox. All glassware was rigorously dried overnight at 160 °C and cooled under vacuum prior to use. Iron and cobalt phthalocyanines (TCI America) were dried under vacuum overnight before being transferred into a glovebox for use and storage. Toluene, tetrahydrofuran (THF), and dimethoxyethane (DME) were distilled from a purple solution of sodium/benzophenone ketyl under nitrogen. Hexanes were distilled from sodium under nitrogen. All other reagents were purchased from commercial sources and used without further purification.

Spectroscopy. NMR spectra were recorded at 294 K, unless otherwise stated, on a 400 MHz Bruker Avance III spectrometer or a 500 MHz Bruker Avance III spectrometer. All ^{1}H NMR shifts are reported relative to the impurity of the internal solvent. Elemental analyses (C, H, N) were performed at Simon Fraser University by Mr. Paul Mulyk on a Carlo Erba EA 1110 CHN elemental analyzer. Samples for elemental analyses were loaded into preweighed tin capsules inside a glovebox, sealed by crimping the capsules with tweezers, removed from the glovebox, weighed, and promptly loaded into the analyzer. UV−visible−NIR solution spectra were recorded on a Varian Cary 5000, Ocean Optics JAZ-LE200-XR1, or a Jasco V-770 spectrophotometer in a 0.1 or 1 cm quartz cell or a 0.1 cm quartz cell equipped with a Kontes PTFE plug, and HI-VAC valve for air-sensitive samples. The MCD spectra were measured with a Jasco J-1500 CD spectrometer using a Jasco MCD-581 electromagnet operated at 1.0 T or a permanent magnet operated at 1.6 T. The completed MCD spectra were measured at 10 °C in parallel and antiparallel orientations with respect to the magnetic field. The MCD spectra were recorded in terms of mDeg = $[\theta]$ on the y-axis and were converted to molar ellipticity via $\Delta\varepsilon = \theta/(32980Blc)$, where B is the magnetic field, l is the path length (cm), and c is the concentration (M).[137] EPR spectra were collected on a Bruker X-band ELEXSYS E-500 instrument at 150 K. Samples were prepared and frozen under a nitrogen atmosphere. ^{57}Fe Mössbauer spectra were recorded with a W.E.B. Research Mössbauer spectroscopy system. All samples were measured at room temperature. A ^{57}Co (in rhodium matrix) source with a strength of ∼40 mCi was used. The detector was a Reuters-Stokes Kr/CO_2 proportional counter. The sample powder was loaded in a high-density polyethylene flat washer and wrapped in Parafilm and Kapton tape inside an inert-atmosphere glovebox and mounted in the Mössbauer sample holder; the wrapped sample was in contact with the atmosphere for under 1 min and was rapidly placed under helium inside the spectrometer. The velocity was scanned between 4 and −4 mm s^{-1} using a constant acceleration triangle waveform and calibrated against Fe foil measured at 295 K in zero magnetic field. All isomer shifts (δ) are relative to Fe foil. Spectra were fit to Lorentzian curves using the program Fityk.[138] Doublet peaks were allowed to refine in peak width but were constrained to have the same area. The doublet assigned to be Fe(II)Pc in the $[FePc]^-$ complex spectra was constrained to the parameters from Fe(II)Pc in the air exposed sample, leading to a negligible difference in the overall fit.

Computational Aspects. All calculations were run using Gaussian 16.[139] BP86[140,141] with Wachter's full-electron basis set[142] (Wf) for iron and the 6-311G(d) basis set[143] for the other atoms was used for all geometry optimizations. Vibrational frequencies were calculated to ensure all geometries were local minima. Taking into consideration an expected exchange−correlation functional dependency on the predicted theoretical energies of the excited states,[144−147] time-dependent density functional theory (TDDFT) with TPSSh[148,149] and TPSS[148] was used to calculate the first 80 excited states of each molecule. In addition, O3LYP,[150] tHCTHThyb,[151] B97-1,[152] B98,[153] M05,[154] and M06[155] functionals were tested in EPR parameter calculations. The same basis sets as for the geometry optimizations were used for the TDDFT and EPR calculations. Mössbauer parameters were calculated using TPSS and TPSSh functionals. DFT and TDDFT calculations were run in either a gas phase or solution using the PCM model,[156] with dichloromethane (DCM) or dimethylformamide (DMF) as the solvent. QMForge[157] was used for the molecular orbital composition analyses.

Single Crystal X-ray Crystallographic Analysis. Crystalline samples were mounted on a 150 mm MiTeGen Dual-Thickness MicroMount using Paratone N oil (Hampton) and data collected at 150 K. Diffraction data was collected using a Bruker Smart Apex II single crystal diffractometer with a TRIUMPH monochromated Mo Kα radiation (λ = 0.71073 Å) source with a crystal-to-detector distance of 50 mm, using a series of θ and ω scans in 0.50° oscillations. The data was processed and corrected for Lorentz and polarization effects and an empirical absorption correction was applied, using the Bruker Apex II software suite.[158] The structures were solved with SIR92,[159,160] and subsequent refinements were performed using the SHELXTL crystallo-

https://doi.org/10.1021/acs.inorgchem.2c03456
Inorg. Chem. 2022, 61, 20177−20199

graphic software package of Bruker-AXS.[161] The coordinates and anisotropic displacement parameters for the non-hydrogen atoms were refined. Hydrogen atoms were placed in idealized geometric positions and linked to their respective carbon atoms using a riding model during refinement. DME molecules were disordered and modeled accordingly. Diagrams were prepared using MERCURY[162] and POV-RAY.[163] Crystallographic data are provided in the Supporting Information and Tables 1 and 2. Additional crystallographic information can be found in CCDC 2205011 and 2205012, respectively.

Synthetic Procedures. *Synthesis of K(DME)$_4$[PcFe] (1).* To a suspension of PcFe (57.0 mg, 0.100 mmol) in 10 mL of DME, 1 equiv of KBEt$_3$H (0.10 mL, 0.100 mmol) was added slowly, causing the solution to become dark purple. After the solution was stirred for 20 h, the solvent was removed *in vacuo*; the residue was washed with 5 mL of toluene and then extracted with 6 mL of DME/2 mL of hexanes. The extracts were filtered through Celite. Purple crystals of K(DME)$_4$[PcFe] (**1**) were isolated in three fractions. Yield: 82 mg (88%). UV−vis: (DME) λ_{max} 326, 509, and 806 nm. Anal. Calcd for $C_{48}H_{56}N_8O_8FeK$: C, 59.56; H, 5.83; N, 11.58. Found C, 59.03; H, 5.82; N, 11.13. ^{1}H NMR (THF-d_8): δ = 16.8 (br s, 8H), 15.8 (br s, 8H) ppm. Crystals suitable for X-ray analysis were grown by layering hexanes onto a DME solution of the product in a capped 1 dram vial.

Synthesis of K(DME)$_4$[PcCo] (2). To a suspension of PcCo (57 mg, 0.100 mmol) in 10 mL of DME, 1 equiv of KBEt$_3$H (0.10 mL, 0.100 mmol) was added slowly, generating a dark green-yellow solution. After the solution was stirred for 20 h, the solvent was removed *in vacuo*; the residue was washed with 5 mL of toluene and then extracted sequentially with 10 mL of DME/2 mL of hexanes. The extracts were filtered through Celite. Black crystals of K(DME)$_4$[PcCo] (**2**) were isolated in two fractions. Yield: 79 mg (81%). UV−vis: (DME) λ_{max} 316, 385, 465, and 664 nm. Anal. Calcd for $C_{44}H_{46}N_8O_6CoK$: C, 59.99; H, 5.26; N, 12.72. Found C, 59.39; H, 4.73; N, 13.03. ^{1}H NMR (THF-d_8): δ = 9.30 (s, 8H), 7.91 (s, 8H) ppm. ^{13}C{^{1}H} NMR (solvent): δ = 155.6, 141.4, 125.9, 120.7, 71.4, 57.8 ppm. Crystals suitable for X-ray analysis were grown by layering hexanes onto a DME solution of the product in a capped 1 dram vial.

■ ASSOCIATED CONTENT

Supporting Information

The Supporting Information is available free of charge at https://pubs.acs.org/doi/10.1021/acs.inorgchem.2c03456.

Additional correlations, experimental, and computational data (PDF)

Accession Codes

CCDC 2205011−2205012 contain the supplementary crystallographic data for this paper. These data can be obtained free of charge via www.ccdc.cam.ac.uk/data_request/cif, or by emailing data_request@ccdc.cam.ac.uk, or by contacting The Cambridge Crystallographic Data Centre, 12 Union Road, Cambridge CB2 1EZ, UK; fax: +44 1223 336033.

■ AUTHOR INFORMATION

Corresponding Authors

Victor N. Nemykin − *Department of Chemistry, University of Tennessee, Knoxville, Tennessee 37996, United States;* orcid.org/0000-0003-4345-0848; Email: vnemykin@utk.edu

Daniel B. Leznoff − *Department of Chemistry, Simon Fraser University, Burnaby, British Columbia V5A 1S6, Canada;* orcid.org/0000-0002-3426-2848; Email: dleznoff@sfu.ca

Authors

Briana R. Schrage − *Department of Chemistry, University of Tennessee, Knoxville, Tennessee 37996, United States*

Wen Zhou − *Department of Chemistry, Simon Fraser University, Burnaby, British Columbia V5A 1S6, Canada*

Laurel A. Harrison − *Department of Chemistry, University of Tennessee, Knoxville, Tennessee 37996, United States*

Dustin E. Nevonen − *Department of Chemistry, University of Tennessee, Knoxville, Tennessee 37996, United States*

John R. Thompson − *Department of Chemistry, Simon Fraser University, Burnaby, British Columbia V5A 1S6, Canada*

Kathleen E. Prosser − *Department of Chemistry, Simon Fraser University, Burnaby, British Columbia V5A 1S6, Canada*

Charles J. Walsby − *Department of Chemistry, Simon Fraser University, Burnaby, British Columbia V5A 1S6, Canada;* orcid.org/0000-0003-3194-8227

Christopher J. Ziegler − *Department of Chemistry, University of Akron, Akron, Ohio 44325, United States;* orcid.org/0000-0002-0142-5161

Complete contact information is available at: https://pubs.acs.org/10.1021/acs.inorgchem.2c03456

Author Contributions

‖B.R.S. and W.Z.: These authors contributed equally.

Notes

The authors declare no competing financial interest.

■ ACKNOWLEDGMENTS

Generous support from the NSF (CHE-2153081), Minnesota Supercomputing Institute, WestGrid Canada, and the University of Tennessee to V.N.N. is greatly appreciated. K.E.P., C.W., and D.B.L. are grateful to NSERC of Canada for generous support of this research via a Vanier Postgraduate Fellowship (K.E.P.) and the Discovery Grants program (C.W., D.B.L.). We want to acknowledge Prof. Karl Kadish for some electrochemical data.

■ REFERENCES

(1) Nemykin, V. N.; Tret'yakova, I. N.; Volkov, S. V.; Li, V. D.; Mekhryakova, N. G.; Kaliya, O. L.; Luk'yanets, E. A. Synthesis, structure and properties of coordination compounds of iron phthalocyanines and their analogues. *Russ. Chem. Rev.* **2000**, *69*, 325−346.

(2) Hanack, M. In *Phthalocyanines: Properties and Applications*; Leznoff, C. C., Lever, A. B. P., Eds.; VCH: 1989; Vol. 2, pp 43−96.

(3) Ercolani, C.; Floris, B. In *Phthalocyanines: Properties and Applications*; Leznoff, C. C., Lever, A. B. P., Eds.; VCH: 1989; Vol. 2, pp 1−43.

(4) Taube, R. New aspects of the chemistry of transition metal phthalocyanines. *Pure Appl. Chem.* **1974**, *38*, 427−438.

(5) Sorokin, A. B. Phthalocyanine Metal Complexes in Catalysis. *Chem. Rev.* **2013**, *113*, 8152−8191.

(6) Kennedy, B. J.; Murray, K. S.; Zwack, P. R.; Homborg, H.; Kalz, W. Spin states in iron(III) phthalocyanines studied by Moessbauer, magnetic susceptibility, and ESR measurements. *Inorg. Chem.* **1986**, *25*, 2539−2545.

(7) L'Her, M.; Pondave, A. In *The Porphyrin Handbook*; Kadish, K. M., Smith, K., Guilard, R., Eds.; Academic Press: 2003, Vol. *16*, pp 117−170.

(8) Afanasiev, P.; Sorokin, A. B. μ- Nitrido Diiron Macrocyclic Platform: Particular Structure for Particular Catalysis. *Acc. Chem. Res.* **2016**, *49*, 583−593.

(9) Woehrle, D.; Baziakina, N.; Suvorova, O.; Makarov, S.; Kutureva, V.; Schupak, E.; Schnurpfeil, G. Phthalocyanine coatings on silica and zinc oxide. Synthesis and their activities in the oxidation of sulfide. *J. Porphyrins Phthalocyanines* **2004**, *08*, 1390−1401.

(10) Woehrle, D.; Suvorova, O.; Gerdes, R.; Bartels, O.; Lapok, L.; Baziakina, N.; Makarov, S.; Slodek, A. Efficient oxidations and photooxidations with molecular oxygen using metal phthalocyanines as catalysts and photocatalysts. *J. Porphyrins Phthalocyanines* **2004**, *08*, 1020−1041.

(11) Cailler, L. P.; Clemancey, M.; Barilone, J.; Maldivi, P.; Latour, J.-M.; Sorokin, A. B. Comparative Study of the Electronic Structures of μ-Oxo, μ- Nitrido, and μ- Carbido Diiron Octapropylporphyrazine Complexes and Their Catalytic Activity in Cyclopropanation of Olefins. *Inorg. Chem.* **2020**, *59*, 1104−1116.
(12) Colomban, C.; Tobing, A. H.; Mukherjee, G.; Sastri, C. V.; Sorokin, A. B.; de Visser, S. P. Mechanism of Oxidative Activation of Fluorinated Aromatic Compounds by N- Bridged Diiron- Phthalocyanine: What Determines the Reactivity? *Chem.—Eur. J.* **2019**, *25*, 14320−14331.
(13) Neu, H. M.; Zhdankin, V. V.; Nemykin, V. N. Binuclear iron(III) phthalocyanine(μ- oxodimer) /tetrabutylammonium oxone: a powerful catalytic system for oxidation of hydrocarbons in organic solution. *Tetrahedron Lett.* **2010**, *51*, 6545−6548.
(14) Neu, H. M.; Yusubov, M. S.; Zhdankin, V. V.; Nemykin, V. N. Binuclear iron(III) phthalocyanine(μ- oxo- dimer) - catalyzed oxygenation of aromatic hydrocarbons with iodosylbenzene sulfate and iodosylbenzene as the oxidants. *Adv. Synth. Catal.* **2009**, *351*, 3168−3174.
(15) Geraskin, I. M.; Luedtke, M. W.; Neu, H. M.; Nemykin, V. N.; Zhdankin, V. V. Organic iodine(V) compounds as terminal oxidants in iron(III) phthalocyanine catalyzed oxidation of alcohols. *Tetrahedron Lett.* **2008**, *49*, 7410−7412.
(16) Griffin, J. R.; Wendell, C. I.; Garwin, J. A.; White, M. C. Catalytic C(sp^3) - H Alkylation via an Iron Carbene Intermediate. *J. Am. Chem. Soc.* **2017**, *139*, 13624−13627.
(17) He, C.; Wu, Z.-Y.; Zhao, L.; Ming, M.; Zhang, Y.; Yi, Y.; Hu, J.-S. Identification of FeN4 as an Efficient Active Site for Electrochemical N_2 Reduction. *ACS Catal.* **2019**, *9*, 7311−7317.
(18) Hu, P.; Tan, M.; Cheng, L.; Zhao, H.; Feng, R.; Gu, W.-J.; Han, W. Bio-inspired iron-catalyzed oxidation of alkylarenes enables late-stage oxidation of complex methylarenes to arylaldehydes. *Nat. Commun.* **2019**, *10*, 2425.
(19) Fitzgerald, J. P.; Lebenson, J. R.; Wang, G.; Yee, G. T.; Noll, B. C.; Sommer, R. D. Iron Tetraanthracenotetraazaporphyrins: Synthesis, Structural Characterization, Ligand Binding Properties, and Unexpected Selectivity of a Bis- "Bowl" Tetraazaporphyrin. *Inorg. Chem.* **2008**, *47*, 4520−4530.
(20) Fitzgerald, J. P.; Haggerty, B. S.; Rheingold, A. L.; May, L.; Brewer, G. A. Iron octaethyltetraazaporphyrins: synthesis, characterization, coordination chemistry, and comparisons to related iron porphyrins and phthalocyanines. *Inorg. Chem.* **1992**, *31*, 2006−2013.
(21) Ona-Burgos, P.; Casimiro, M.; Fernandez, I.; Navarro, A. V.; Fernandez-Sanchez, J. F.; Carretero, A. S.; Gutierrez, A. F. Octahedral iron(II) phthalocyanine complexes: multinuclear NMR and relevance as NO_2 chemical sensors. *Dalton Trans.* **2010**, *39*, 6231−6238.
(22) Valero-Navarro, A.; Fernandez-Sanchez, J. F.; Segura-Carretero, A.; Spichiger-Keller, U. E.; Fernandez-Gutierrez, A.; Ona, P.; Fernandez, I. Iron- phthalocyanine complexes immobilized in nanostructured metal oxide as optical sensors of NOx and CO - NMR and photophysical studies. *J. Porphyrins Phthalocyanines* **2009**, *13*, 616−623.
(23) Fernandez-Sanchez, J. F.; Fernandez, I.; Steiger, R.; Beer, R.; Cannas, R.; Spichiger-Keller, U. E. Second- generation nanostructured metal oxide matrices to increase the thermal stability of CO and NO_2 sensing layers based on iron(II) phthalocyanine. *Adv. Functional Mater.* **2007**, *17*, 1188−1198.
(24) Govan, J.; Abarca, G.; Aliaga, C.; Sanhueza, B.; Orellana, W.; Cardenas-Jiron, G.; Zagal, J. H.; Tasca, F. Influence of cyano substituents on the electron density and catalytic activity towards the oxygen reduction reaction for iron phthalocyanine. The case for Fe(II) 2, 3, 9, 10, 16, 17, 23, 24- octa(cyano) phthalocyanine. *Electrochem. Commun.* **2020**, *118*, 106784.
(25) Praats, R.; Kaarik, M.; Kikas, A.; Kisand, V.; Aruvali, J.; Paiste, P.; Merisalu, M.; Leis, J.; Sammelselg, V.; Zagal, J. H.; et al. Electrocatalytic oxygen reduction reaction on iron phthalocyanine-modified carbide-derived carbon/carbon nanotube composite electrocatalysts. *Electrochim. Acta* **2020**, *334*, 135575.
(26) Recio, F. J.; Gutierrez, C. A.; Venegas, R.; Linares-Flores, C.; Caro, C. A.; Zagal, J. H. Optimization of the electrocatalytic activity of MN4- macrocyclics adsorbed on graphite electrodes for the electrochemical oxidation of L- cysteine by tuning the M (II) /(I) formal potential of the catalyst: an overview. *Electrochim. Acta* **2014**, *140*, 482−488.
(27) Kuznetsova, N. A.; Kaliya, O. L. Heterogenized metallophthalocyanines for photodynamic microorganism inactivation: an overview of our experience. *Makrogeterotsikly* **2015**, *8*, 8−19.
(28) Gerasimova, G. K.; Yakubovskaya, R. I.; Pankratov, A. A.; Treshchalina, E. M.; Nemtsova, E. R.; Andreeva, T. N.; Venediktova, Yu. B.; Plyutinskaya, A. D.; Bezborodova, O. A.; Sidorova, T. A.; Baryshnikov, A. B.; Kaliya, O. L.; Voroztsov, G. N.; Luzhkov, Yu. M. Binary catalytic therapy: A new approach to treatment of malignant tumors. Results of pre- clinical and clinical studies. *Russ. J. Gen. Chem.* **2015**, *85*, 289−302.
(29) Nxele, S. R.; Nyokong, T. Conjugation of Azide- functionalised CdSe /ZnS Quantum Dots with Tetrakis(5- hexyn- oxy) Fe(II) phthalocyanine via Click Chemistry for Electrocatalysis. *Electrochim. Acta* **2016**, *194*, 26−39.
(30) Nxele, S. R.; Mashazi, P.; Nyokong, T. Electrode Modification Using Alkynyl Substituted Fe(II) Phthalocyanine via Electrografting and Click Chemistry for Electrocatalysis. *Electroanalysis* **2015**, *27*, 2468−2478.
(31) Maringa, A.; Mashazi, P.; Nyokong, T. Characterization of electrodes modified by one pot or step by step electro- click reaction and axial ligation of iron tetracarboxyphthalocyanine. *Electrochim. Acta* **2014**, *145*, 237−244.
(32) Coates, M.; Nyokong, T. Characterization of glassy carbon electrodes modified with carbon nanotubes and iron phthalocyanine through grafting and click chemistry. *Electrochim. Acta* **2013**, *91*, 158−165.
(33) Watkins, J. J.; Balch, A. L. Complexes of ferrous phthalocyanine with aromatic nitroso compounds, isocyanides, and phosphites. *Inorg. Chem.* **1975**, *14*, 2720−2723.
(34) Dale, B. W.; Williams, R. J. P.; Edwards, P. R.; Johnson, C. E. Mössbauer spectra of compounds containing iron(II) in strong- field tetragonal environments. *Trans. Faraday Soc.* **1968**, *64*, 620−629.
(35) Dale, B. W.; Williams, R. J. P. Nature of electric field-gradient tensor in strong-field tetragonal and pseudo-tetragonal complexes of divalent iron. *Trans. Faraday Soc.* **1968**, *64*, 3011−3013.
(36) Dale, B. W. Effect of axial ligands on the electronic absorption spectrum of phthalocyanineiron(II). *Trans. Faraday Soc.* **1969**, *65*, 331−339.
(37) Hanack, M.; Hirsch, A. Synthesis of bridged mixed valence macrocyclic compounds. *Synth. Met.* **1989**, *29*, 9−13.
(38) Nemykin, V. N.; Polshina, A. E.; Chernii, V. Y.; Polshin, E. V.; Kobayashi, N. Synthesis, properties and Mossbauer spectra of bisaxially co- ordinated iron(II) phthalocyanine low- spin complexes: the first semi- quantitative explanation of the influence of the character of axial ligands on the spectral parameters. *Dalton* **2000**, 1019−1025.
(39) Nemykin, V. N.; Kobayashi, N.; Chernii, V. Y.; Belsky, V. K. Mossbauer, crystallographic, and density functional theoretical investigation of the electronic structure of bis- ligated low- spin iron(II) phthalocyanines. *Eur. J. Inorg. Chem.* **2001**, *2001*, 733−743.
(40) Fernandez, I.; Pregosin, P. S.; Albinati, A.; Rizzato, S.; Spichiger-Keller, U. E.; Nezel, T.; Fernandez-Sanchez, J. F. Solution NMR and X-ray structural studies on phthalocyaninatoiron complexes. *Helv. Chim. Acta* **2006**, *89*, 1485−1496.
(41) Nevonen, D. E.; Ferch, L. S.; Chernii, V. Y.; Herbert, D. E.; van Lierop, J.; Nemykin, V. N. X- Ray structures, Mossbauer hyperfine parameters, and molecular orbital descriptions of the phthalocyaninato iron(II) azole complexes. *J. Porphyrins Phthalocyanines* **2020**, *24*, 894−903.
(42) Ettorre, R.; Marton, D.; Russo, U.; Zanonato, P. Complexes of phthalocyaninatoiron(II) with diazoles. *J. Porphyrins Phthalocyanines* **2001**, *05*, 545−547.
(43) Ouedraogo, G. V.; More, C.; Richard, Y.; Benlian, D. Charge-transfer and Moessbauer spectra of axially substituted iron phthalocyanines. *Inorg. Chem.* **1981**, *20*, 4387−4393.

https://doi.org/10.1021/acs.inorgchem.2c03456
Inorg. Chem. 2022, 61, 20177−20199

(44) Ough, E. A.; Stillman, M. J. Analysis of the absorption and magnetic circular dichroism spectra of iron(II) phthalocyanine. *Inorg. Chem.* **1994**, *33*, 573−583.
(45) Stillman, M. J.; Thomson, A. J. Orbital reduction factors in the lowest excited state of the phthalocyanine ring and their measurement by magnetic circular dichroism spectroscopy. *J. Chem. Soc., Faraday Trans. 2* **1974**, *70*, 805−814.
(46) Hanack, M.; Deger, S.; Lange, A. Bisaxially coordinated macrocyclic transition metal complexes. *Coord. Chem. Rev.* **1988**, *83*, 115−136.
(47) Schneider, O.; Hanack, M. Axially polymerized (phthalocyaninato) iron(II) with pyrazine, 4, 4'- bipyridine, 1, 4- diisocyanobenzene, or 1, 4- diazabicyclo[2.2.2] octane as bridging ligands; synthesis, characterization, and electrical conductivities. *Chem. Ber.* **1983**, *116*, 2088−2108.
(48) Hanack, M.; Hirsch, A.; Lehmann, H. Soluble oligomeric bridged phthalocyaninatoiron(II) complexes. *Angew. Chem., Int. Ed.* **1990**, *29*, 1467−1468.
(49) Hanack, M.; Duerr, K.; Lange, A.; Osio Barcina, J.; Pohmer, J.; Witke, E. Synthesis of low band gap polymers - a challenge for organic chemists. *Synth. Met.* **1995**, *71*, 2275−2278.
(50) Hanack, M. Intrinsic semiconducting materials on phthalocyanine basis. *Turk. J. Chem.* **1998**, *22*, 13−22.
(51) Hanack, M.; Fiedler, M.; Subramanian, L. R. Phthalocyaninatoiron complexes with tridentate ligands. *Synth. Met.* **1999**, *100*, 123−130.
(52) Bayo, K.; Ouedraogo, G. V.; Terzian, G.; Benlian, D. UV- visible and IR spectra of iron(II) phthalocyanine polymer complexes linked by bis- pyridinato ligands. *Polyhedron* **1990**, *9*, 1087−1090.
(53) Ercolani, C.; Monacelli, F.; Dzugan, S.; Goedken, V. L.; Pennesi, G.; Rossi, G. X- ray crystal structure of μ- oxo- bis[(1- methylimidazole) phthalocyaninatoiron(III)] and comments on the molecular structure and chemistry of oxo- bridged iron phthalocyaninate dimers. *J. Chem. Soc., Dalton Trans.* **1991**, 1309−1315.
(54) Janczak, J.; Kubiak, R. Pyrazine control of the supramolecular chemistry of iron(II) and cobalt (II) phthalocyanines. *CrystEngComm* **2010**, *12*, 3599−3606.
(55) Ohya, T.; Morohoshi, H.; Sato, M. Preparation and characterization of low- spin iron(II) porphyrin complexes with bis(phosphine) or bis(phosphite) axial ligands. *Inorg. Chem.* **1984**, *23*, 1303−1305.
(56) Sweigart, D. A. Axial ligand substitution in iron(II) phthalocyanine adducts: replacement of tri- n- butyl phosphite by tri- n- butylphosphine. *J. Chem. Soc., Dalton Trans.* **1976**, 1476−1477.
(57) Nemykin, V. N.; Nevonen, D. E.; Osterloh, W. R.; Ferch, L. S.; Harrison, L. A.; Marx, B. S.; Kadish, K. M. Application of Lever's E_L Parameter Scale toward Fe(II)/Fe(III) versus Pc(2-)/Pc(1-) Oxidation Process Crossover Point in Axially Coordinated Iron(II) Phthalocyanine Complexes. *Inorg. Chem.* **2021**, *60*, 16626−16644.
(58) Zanguina, A.; Bayo-Bangoura, M.; Bayo, K.; Ouedraogo, G. V. IR and UV- visible spectra of iron(II) phthalocyanine complexes with phosphine or phosphite. *Bull. Chem. Soc. Ethiopia* **2002**, *16*, 73−79.
(59) Nemykin, V. N.; Nevonen, D. E.; Ferch, L. S.; Shepit, M.; Herbert, D. E.; van Lierop, J. Accurate Prediction of Mössbauer Hyperfine Parameters in Bis- Axially Coordinated Iron(II) Phthalocyanines Using Density Functional Theory Calculations: A Story of a Single Orbital Revealed by Natural Bond Orbital Analysis. *Inorg. Chem.* **2021**, *60*, 3690−3706.
(60) Anderson, D. R.; Solntsev, P. V.; Rhoda, H. M.; Nemykin, V. N. How big is big? Separation by conventional methods, X- ray and electronic structures of positional isomers of bis- tert- butylisocyano adduct of 2(3), 9(10), 16(17), 23(24) - tetrachloro- 3(2), 10(9), 17(16), 24(23) - tetra(2, 6- di- iso- propylphenoxy) - phthalocyaninato iron(II) complex. *J. Porphyrins Phthalocyanines* **2016**, *20*, 337−351.
(61) Nemykin, V. N.; Purchel, A. A.; Spaeth, A. D.; Barybin, M. V. Probing the Electronic Properties of a Trinuclear Molecular Wire Involving Isocyanoferrocene and Iron(II) Phthalocyanine Motifs. *Inorg. Chem.* **2013**, *52*, 11004−11012.
(62) Hanack, M.; Knecht, S.; Polley, R.; Subramanian, L. R. Axially 1, 4- diisocyanobenzene bridged substituted iron(II) phthalocyanines and 2, 3- naphthalocyanines. *Synth. Met.* **1996**, *80*, 183−189.
(63) Schmid, G.; Witke, E.; Schlick, U.; Knecht, S.; Hanack, M. Substituent effects in soluble phthalocyaninatoiron(II) complexes. *J. Mater. Chem.* **1995**, *5*, 855−859.
(64) Ryu, H.; Knecht, S.; Subramanian, L. R.; Hanack, M. Synthesis and properties of bridged phthalocyaninatoiron(II) complexes with bidentate aliphatic isocyanides. *Synth. Met.* **1995**, *72*, 289−296.
(65) Hanack, M.; Knecht, S.; Witke, E.; Haisch, P. Synthesis and properties of soluble metallophthalocyanines. *Synth. Met.* **1993**, *55*, 873−878.
(66) Hanack, M.; Lange, A.; Grosshans, R. Tetrazine- bridged phthalocyaninato- metal complexes as semiconducting material. *Synth. Met.* **1991**, *45*, 59−70.
(67) Calderazzo, F.; Frediani, S.; James, B. R.; Pampaloni, G.; Reimer, K. J.; Sams, J. R.; Serra, A. M.; Vitali, D. Synthesis and Moessbauer spectroscopic studies of carbonyl derivatives of (phthalocyaninato) iron(II). *Inorg. Chem.* **1982**, *21*, 2302−2306.
(68) Calderazzo, F.; Pampaloni, G.; Vitali, D.; Collamati, I.; Dessy, G.; Fares, V. Bis adducts of phthalocyaninatoiron(II) with Group 6A axial donor atoms. Crystal and molecular structure of sulfur- bonded bis(dimethyl sulfoxide) phthalocyaninatoiron(II) - dimethyl sulfoxide (1 /2). *J. Chem. Soc., Dalton Trans.* **1980**, 1965−1969.
(69) Calderazzo, F.; Vitali, D.; Pampaloni, G.; Collamati, I. Reaction of pentacarbonyliron with phthalonitrile in dimethylformamide and isolation of carbonyl derivatives of iron(II) phthalocyanine stabilized by group 6 donor atoms. *J. Chem. Soc., Chem. Commun.* **1979**, 221b−222.
(70) Calderazzo, F.; Pampaloni, G.; Vitali, D.; Pelizzi, G.; Collamati, I.; Frediani, S.; Serra, A. M. Carbonyl derivatives of phthalocyaninatoiron(II), especially those containing Group VI axial donor atoms. Crystal and molecular structure of carbonyl(N, N-dimethylformamide) phthalocyaninatoiron(II) and Moessbauer studies of some of the products. *J. Organomet. Chem.* **1980**, *191*, 217−242.
(71) Lever, A. B. P.; Wilshire, J. P. Electrochemistry of iron phthalocyanine complexes in nonaqueous solvents and the identification of five- coordinate iron(I) phthalocyanine derivatives. *Inorg. Chem.* **1978**, *17*, 1145−1151.
(72) Jones, J. G.; Twigg, M. V. Axial ligand dissociation of phthalocyaninatoiron(II) adducts. Further evidence for a dissociative mechanism of substitution. *J. Chem. Soc., Dalton Trans.* **1978**, 1709−1714.
(73) Beck, A.; Mangold, K. M.; Hanack, M. Soluble (tetraethylphthalocyaninato)iron(II) and -cobalt(II) compounds. *Chem. Ber.* **1991**, *124*, 2315−2321.
(74) Dieing, R.; Schmid, G.; Witke, E.; Feucht, C.; Dressen, M.; Pohmer, J.; Hanack, M. Soluble substituted μ-oxo(phthalocyaninato)-iron(III) dimers. *Chem. Ber.* **1995**, *128*, 589−598.
(75) Kobayashi, N.; Shirai, H.; Hojo, N. Iron(III) phthalocyanines: oxidation and spin states of iron in iron phthalocyanines with carboxyl groups. *J. Chem. Soc., Dalton Trans.* **1984**, 2107−2110.
(76) Sievertsen, S.; Murray, K. S.; Moubaraki, B.; Berry, K. J.; Korbatieh, Y.; Cashion, J. D.; Brown, L. J.; Homborg, H. Dimeric low-spin iron(III) phthalocyanines: synthesis and properties of ferromagnetically coupled μ-oxodi(acidophthalocyaninatoferrates(III)). *Z. Anorg. Allg. Chem.* **1994**, *620*, 1203−1212.
(77) Bakshi, E. N.; Murray, K. S. Applied field Moessbauer spectra of low-spin mononuclear and binuclear iron(III)-phthalocyanines. *Hyperfine Interact.* **1988**, *40*, 283−286.
(78) Clack, D. W.; Yandle, J. R. Electronic spectra of the negative ions of some metal phthalocyanines. *Inorg. Chem.* **1972**, *11*, 1738−1742.
(79) Clack, D. W.; Hush, N. S.; Yandle, J. R. The ESR spectra of metal phthalocyanine negative ions. *Chem. Phys. Lett.* **1967**, *1*, 157−159.
(80) Kadish, K. M.; Bottomley, L. A.; Cheng, J. S. Electrochemical characterization of iron(II) and iron(I) phthalocyanine-amine derivatives. *J. Am. Chem. Soc.* **1978**, *100*, 2731−2737.
(81) Arici, M.; Arican, D.; Ugur, A. L.; Erdogmus, A.; Koca, A. Electrochemical and spectroelectrochemical characterization of newly synthesized manganese, cobalt, iron and copper phthalocyanines. *Electrochim. Acta* **2013**, *87*, 554−566.
(82) Gunay, I.; Orman, E. B.; Altindal, A.; Salih, B.; Ozer, M.; Ozkaya, A. R. Novel tetrakis 4-(hydroxymethyl)-2,6-dimethoxyphenoxyl

https://doi.org/10.1021/acs.inorgchem.2c03456
Inorg. Chem. 2022, 61, 20177−20199

substituted metallophthalocyanines: synthesis, electrochemical redox, electrocatalytic oxygen reducing, and volatile organic compounds sensing and adsorption properties. *Dyes Pigments* **2018**, *154*, 172−187.
(83) Demirbas, U.; Akyuz, D.; Akcay, H. T.; Koca, A.; Mentese, E.; Kantekin, H. Novel 1,2,4-triazole substituted metallo-phthalocyanines: synthesis, characterization and investigation of electrochemical and spectroelectrochemical properties. *J. Mol. Struct.* **2018**, *1173*, 205−212.
(84) Demirbas, U.; Akyuz, D.; Mermer, A.; Akcay, H. T.; Demirbas, N.; Koca, A.; Kantekin, H. The electrochemical and spectroelectrochemical properties of metal free and metallophthalocyanines containing triazole/piperazine units. *Spectrochim. Acta* **2016**, *153A*, 478−487.
(85) Konarev, D. V.; Kuzmin, A. V.; Ishikawa, M.; Nakano, Y.; Faraonov, M. A.; Khasanov, S. S.; Otsuka, A.; Yamochi, H.; Saito, G.; Lyubovskaya, R. N. Layered salts with iron hexadecachlorophthalocyanine anions − the formation of $[\{FeCl_{16}Pc\}_2]^{3-}$ dimers containing $[Fe^{I}Cl_{16}Pc(2-)]^{-}$ and diamagnetic $[Fe^{\circ}Cl_{16}Pc(2-)]^{2-\alpha}$. *Eur. J. Inorg. Chem.* **2014**, *2014*, 3863−3870.
(86) Konarev, D. V.; Ishikawa, M.; Khasanov, S. S.; Otsuka, A.; Yamochi, H.; Saito, G.; Lyubovskaya, R. N. Synthesis, structural and magnetic properties of ternary complexes of $(Me_4P^+).\{[Fe(I)Pc(-2)]^-\}$.tripticene and $(Me_4P^+).\{[Fe(I)Pc(-2)]^-\}.(N,N,N'N'$-tetrabenzyl-p-phenylendiamine$)_{0.5}$ with iron(I) phthalocyanine anions. *Inorg. Chem.* **2013**, *52*, 3851−3859.
(87) Konarev, D. V.; Kuzmin, A. V.; Khasanov, S. S.; Lyubovskaya, R. N. Zwitterionic $\{Fe(I)Pc(-2)\}.(TMP^+)$ assemblies comprising anionic iron(I) phthalocyanines and coordinating N,N,N'-trimethylpiperazinium cations. *Dalton Trans.* **2013**, *42*, 9870−9876.
(88) Konarev, D. V.; Kuzmin, A. V.; Simonov, S. V.; Khasanov, S. S.; Otsuka, A.; Yamochi, H.; Saito, G.; Lyubovskaya, R. N. Ionic compound containing iron phthalocyanine $(Fe^{I}Pc)^-$ anions and $(C70^-)_2$ dimers. Optical and magnetic properties of $(Fe^{I}Pc)^-$ in the solid state. *Dalton Trans.* **2012**, *41*, 13841−13847.
(89) Tasso, T. T.; Furuyama, T.; Kobayashi, N. Absorption and electrochemical properties of cobalt and iron phthalocyanines and their quaternized derivatives: aggregation equilibrium and oxygen reduction electrocatalysis. *Inorg. Chem.* **2013**, *52*, 9206−9215.
(90) (a) Nevonen, D. E.; Rohde, G. T.; Nemykin, V. N. New Insight Into an Old Problem: Analysis, Interpretation, and Theoretical Modeling of the Absorption and Magnetic Circular Dichroism Spectra of Monomeric and Dimeric Zinc Phthalocyanine Cation-Radical. *Inorg. Chem.* **2019**, *58*, 14120−14135. (b) McKearney, D.; Choua, S.; Zhou, W.; Ganga-Sah, Y.; Ruppert, R.; Wytko, J.; Weiss, J.; Leznoff, D. B. Ring-oxidized Zinc(II) phthalocyanine cations: Structure, spectroscopy and decomposition behavior. *Inorg. Chem.* **2018**, *57*, 9644−9655.
(91) Tahiri, M.; Doppelt, P.; Fischer, J.; Weiss, R. Synthesis and molecular structure of kryptofix 222 potassium phthalocyaninatoferrate, [K⊂222][FePc], and (18-crown-6)(tetrahydrofuran)lithium phthalocyaninatoferrate, [Li⊂18c.6][Li(THF)⊂18c.6][FePc]. *Inorg. Chim. Acta* **1987**, *127*, L1−L3.
(92) Konarev, D. V.; Khasanov, S. S.; Lyubovskaya, R. N. Fullerene complexes with coordination assemblies of metalloporphyrins and metal phthalocyanines. *Coord. Chem. Rev.* **2014**, *262*, 16−36.
(93) Konarev, D. V.; Zorina, L. V.; Khasanov, S. S.; Hakimova, E. U.; Lyubovskaya, R. N. Structure and magnetic properties of ionic compound $(Cp^*_2Cr^+)\bullet(Fe^{I}Pc^-)\bullet(C_6H_4Cl_2)_4$ containing negatively charged iron phthalocyanine. *New J. Chem.* **2012**, *36*, 48−51.
(94) Kaczmarzyk, T.; Jackowski, T.; Dzilinski, K. Spectroscopic characteristics of Fe^{I}-phthalocyanine. *Nucleonika* **2007**, *52*, S99−S103.
(95) Zhou, W.; McKearney, D.; Leznoff, D. B. Structural diversity of F-element monophthalocyanine complexes. *Chem.—Eur. J.* **2020**, *26*, 1027−1031.
(96) Wong, E. W.; Leznoff, D. B. Synthesis and structural characterization of a magnesium phthalocyanine(3-) anion. *J. Porphyrins Phthalocyanines* **2012**, *16*, 154−162.
(97) Zhou, W.; Thompson, J. R.; Leznoff, C. C.; Leznoff, D. B. The redox active Chromium Phthalocyanine system: Isolation of five oxidation states from $Pc^{4-}Cr(I)$ to $Pc^{2-}Cr(III)$. *Chem.—Eur. J.* **2017**, *23*, 2323−2331.
(98) Nevonen, D. E.; Ferch, L. S.; Schrage, B. R.; Nemykin, N. V. Charge-transfer spectroscopy of bisaxially coordinated iron(II) phthalocyanines through the prism of the Lever's E_L parameters scale, MCD spectroscopy, and TDDFT calculations. *Inorg. Chem.* **2022**, *61*, 8250−8266.
(99) Mack, J.; Stillman, M. J. Photochemical formation of the anion radical of zinc phthalocyanine and analysis of the absorption spectrum and magnetic circular dichroism spectral data. Assignment of the optical spectrum of $[ZnPc(-3)]^-$. *J. Am. Chem. Soc.* **1994**, *116*, 1292−1304.
(100) Mack, J.; Stillman, M. J. Assignment of the optical spectrum of metal porphyrin and phthalocyanine radical anions. *J. Porphyrins Phthalocyanines* **2001**, *05*, 67−76.
(101) Keizer, S. P.; Mack, J.; Bench, B. A.; Gorun, S. M.; Stillman, M. J. Spectroscopy and electronic structure of electron deficient zinc phthalocyanines. *J. Am. Chem. Soc.* **2003**, *125*, 7067−7085.
(102) Mason, R.; Williams, G. A.; Fielding, P. E. Structural chemistry of phthalocyaninatocobalt(II) and -manganese(II). *J. Chem. Soc., Dalton Trans.* **1979**, 676−683.
(103) Hückstädt, H.; Homborg, H. Syntheses and properties of phthalocyaninato(2-)metalates(I) of cobalt, rhodium, and iridium. Crystal structure of tetrabutylammonium phthalocyaninato(2-)-cobaltate(I) acetone solvate. *Z. Anorg. Allg. Chem.* **1998**, *624*, 715−720.
(104) Kirner, J. F.; Dow, W.; Scheidt, W. R. Molecular stereochemistry of two intermediate-spin complexes. Iron(II) phthalocyanine and manganese(II) phthalocyanine. *Inorg. Chem.* **1976**, *15*, 1685−1690.
(105) Janczak, J.; Kubiak, R. Stereochemistry and properties of the M(II)-N(py) coordination bond in the low-spin dipyridinated iron(II) and cobalt(II) phthalocyanines. *Inorg. Chim. Acta* **2003**, *342*, 64−76.
(106) Cissell, J. A.; Vaid, T. P.; Yap, G. P. A. Reversible oxidation state change in germanium(tetraphenylporphyrin) induced by a dative ligand: Aromatic $Ge^{II}(TPP)$ and Antiaromatic $Ge^{IV}(TPP)(pyridine)_2$. *J. Am. Chem. Soc.* **2007**, *129*, 7841−7847.
(107) Wong, E. W. Y.; Walsby, C. J.; Storr, T.; Leznoff, D. B. Phthalocyanine as a chemically inert, redox-active ligand: Structural and electronic properties of a Nb(IV)-oxo complex incorporating a highly-reduced phthalocyanine(4-) anion,. *Inorg. Chem.* **2010**, *49*, 3343−3350.
(108) Zhou, W.; Platel, R.; Teixeira Tasso, T.; Furuyama, T.; Kobayashi, N.; Leznoff, D. B. Reducing Zirconium(IV) phthalocyanines and the structure of a $Pc^{4-}Zr$ complex,. *Dalton Trans.* **2015**, *44*, 13955−13961.
(109) Cissell, J. A.; Vaid, T. P.; Rheingold, A. L. Aluminum tetraphenylporphyrin and aluminum phthalocyanine neutral radicals. *Inorg. Chem.* **2006**, *45*, 2367−2369.
(110) Konarev, D. V.; Kuzmin, A. V.; Faraonov, M. A.; Ishikawa, M.; Khasanov, S. S.; Nakano, Y.; Otsuka, A.; Yamochi, H.; Saito, G.; Lyubovskaya, R. M. Synthesis, structures, and properties of crystalline salts with radical anions of metal-containing and metal-free phthalocyanines. *Chem.—Eur. J.* **2015**, *21*, 1014−1028.
(111) Hanack, M.; Linge, A.; Rein, M.; Behnisch, R.; Renz, G.; Leverenz, A. Bridged macrocyclic transition metal complexes as semiconducting materials. *Synth. Met.* **1989**, *29*, 1−8.
(112) Kadish, K. M. Private communication.
(113) Clack, D. W.; Hush, N. S.; Woolsey, I. S. Reduction potentials of some metal phthalocyanines. *Inorg. Chim. Acta* **1976**, *19*, 129−132.
(114) Stillman, M. J.; Thomson, A. J. Assignment of the charge-transfer bands in some metal phthalocyanines. Evidence for the S = 1 state of iron(II) phthalocyanine in solution. *J. Chem. Soc. Faraday Trans. 2* **1974**, *70*, 790−804.
(115) Stillman, M. J.; Thomson, A. J. Orbital reduction factors in the lowest excited state of the phthalocyanine ring and their measurement by magnetic circular dichroism spectroscopy. *J. Chem. Soc. Faraday Trans. 2* **1974**, *70*, 805−814.
(116) Labarta, A.; Molins, E.; Vinas, X.; Tejada, J.; Caubet, A.; Alvarez, S. Electronic structure determination of iron(II) phthalocyanine via magnetic susceptibility and Moessbauer measurements. *J. Phem. Phys.* **1984**, *80*, 444−448.

https://doi.org/10.1021/acs.inorgchem.2c03456
Inorg. Chem. 2022, 61, 20177−20199

(117) Dale, B. W.; Williams, R. J. P.; Edwards, R. P.; Johnson, C. E. S = 1 spin state ofdivalent iron. II. A Mössbauer-effect study on phthalocyanine iron II. *J. Chem. Phys.* **1968**, *49*, 3445−3449.
(118) Kennedy, B. J.; Murray, K. S.; Zwack, P. R.; Homborg, H.; Kalz, W. μ-Oxo iron(III) phthalocyanine. Electronic structure of the solid form obtained from a dihydroxoiron(III) precursor. *Inorg. Chem.* **1985**, *24*, 3302−3305.
(119) Ercolani, C.; Gardini, M.; Murray, K. S.; Pennesi, G.; Rossi, G. Crystalline isomerism in (μ-oxo)bis[(phthalocyaninato)iron(III)]: Further characterization of the isomer having a linear or quasi-linear Fe-O-Fe bond system (μ-oxo(2)). *Inorg. Chem.* **1986**, *25*, 3972−3976.
(120) Gütlich, P.; Bill, E.; Trautwein, A. X.*Mössbauer Spectroscopy and Transition Metal Chemistry*; Springer-Verlag: Berlin, 2011; 569 pp.
(121) Gütlich, P.; Link, R.; Trautwein, A.*Mössbauer Spectroscopy and Transition Metal Chemistry*; Springer: New York, 1978; 280 pp.
(122) Lever, A. B. P.*Inorganic Electronic Spectroscopy*; Elsevier: 1984.
(123) *Inorganic Electronic Structure and Spectroscopy*; Solomon, E. I., Lever, A. B. P., Eds.; Wiley: 1999; Vol. *1*.
(124) Dale, B. W.; Williams, R. J. P.; Johnson, C. E.; Thorp, T. L. S = 1 Spin State of Divalent Iron. I. Magnetic Properties of Phthalocyanine Iron (II). *J. Chem. Phys.* **1968**, *49*, 3441−3444.
(125) Dale, B. W. Evidence from Mössbauer spectroscopy of a departure from tetragonal symmetry in the phthalocyanineiron (II) molecule. *Mol. Phys.* **1974**, *28*, 503−511.
(126) Labarta, A.; Molins, E.; Vinas, X.; Tejada, J.; Caubet, A.; Alvarez, S. Electronic structure determination of iron(II) phthalocyanine via magnetic susceptibility and Mössbauer measurements. *J. Chem. Phys.* **1984**, *80*, 444−448.
(127) Liao, M.-S.; Scheiner, S. Electronic structure and bonding in metal phthalocyanines, Metal = Fe, Co, Ni, Cu, Zn, Mg. *J. Chem. Phys.* **2001**, *114*, 9780−9791.
(128) Van Caemelbecke, E.; Will, S.; Autret, M.; Adamian, V. A.; Lex, J.; Gisselbrecht, J.-P.; Gross, M.; Vogel, E.; Kadish, K. M. Electrochemical and Spectral Characterization of Iron Corroles in High and Low Oxidation States: First Structural Characterization of an Iron(IV) Tetrapyrrole pi Cation Radical. *Inorg. Chem.* **1996**, *35*, 184−192.
(129) Rutter, R.; Hager, L. P.; Dhonau, H.; Hendrich, M. P.; Valentine, M.; Debrunner, P. Chloroperoxidase Compound I: Electron paramagnetic resonance and Mössbauer studies. *Biochemistry* **1984**, *23*, 6809−6816.
(130) Schulz, C. E.; Rutter, R.; Sage, J. T.; Debrunner, P. G.; Hager, L. P. Mössbauer and electron paramagnetic resonance studies of horseradish peroxidase and its catalytic intermediates. *Biochemistry,* **1984**, *23*, 4743−4754.
(131) Schunemann, V.; Jung, C.; Terner, J.; Trautwein, A. X.; Weiss, R. Spectroscopic studies of peroxyacetic acid reaction intermediates of cytochrome P450cam and chloroperoxidase. *J. Inorg. Biochem.* **2002**, *91*, 586−596.
(132) Jayaraj, K.; Gold, A.; Austin, R. N.; Mandón, D.; Weiss, R.; Terner; Bill, J. E.; Müther, M.; Trautwein, A. X. Compound I and II Analogues of a Chlorin. *J. Am. Chem. Soc.* **1995**, *117*, 9079−9080.
(133) Jayaraj, K.; Terner, J.; Gold, A.; Roberts, D. A.; Austin, R. N.; Mandon, D.; Weiss, R.; Bill, E.; Muther, M.; Trautwein, A. X. Influence of Meso Substituents on Electronic States of (Oxoferryl)porphyrin π-Cation Radicals. *Inorg. Chem.* **1996**, *35*, 1632−1640.
(134) Jayaraj, K.; Gold, A.; Austin, R. N.; Ball, L. M.; Terner, J.; Mandon, D.; Weiss, R.; Fischer, J.; DeCian, A.; Bill, E.; Muther, M.; Schunemann, V.; Trautwein, A. X. Compound I and Compound II Analogues from Porpholactones. *Inorg. Chem.* **1997**, *36*, 4555−4566.
(135) Ayougou, K.; Mandon, D.; Fischer, J.; Weiss, R.; Muther, M.; Schunemann, V.; Trautwein, A. X.; Bill, E.; Terner, J.; Jayaraj, K.; Gold, A.; Austin, R. N. Molecular Structure of the Chloroiron(III) Derivative of the meso-Unsubstituted 2,7,12,17-Tetramethyl-3,8,13,18-tetramesitylporphyrin and Weak Ferromagnetic Exchange Interactions in the A_{1u} Oxoiron(IV) Porphyrin Radical Cation Complex. *Chem.—Eur. J.* **1996**, *2*, 1159−1163.
(136) Nemykin, V. N.; Hadt, R. G. Influence of Hartree-Fock Exchange on the Calculated Mössbauer Isomer Shifts and Quadrupole Splittings in Ferrocene Derivatives Using Density Functional Theory,. *Inorg. Chem.* **2006**, *45*, 8297−8307.
(137) Galinato, M. G. I.; Spolitak, T.; Ballou, D. P.; Lehnert, N. Elucidating the Role of the Proximal Cysteine Hydrogen-Bonding Network in Ferric Cytochrome P450cam and Corresponding Mutants Using Magnetic Circular Dichroism Spectroscopy. *Biochemistry* **2011**, *50*, 1053−1069.
(138) Wojdyr, M. Fityk "A general-purpose peak fitting program". *J. Appl. Crystallogr.* **2010**, *43*, 1126−1128.
(139) Frisch, M. J.; Trucks, G. W.; Schlegel, H. B.; Scuseria, G. E.; Robb, M. A.; Cheeseman, J. R.; Scalmani, G.; Barone, V.; Petersson, G. A.; Nakatsuji, H.; Li, X.; Caricato, M.; Marenich, A. V.; Bloino, J.; Janesko, B. G.; Gomperts, R.; Mennucci, B.; Hratchian, H. P.; Ortiz, J. V.; Izmaylov, A. F.; Sonnenberg, J. L.; Williams-Young, D.; Ding, F.; Lipparini, F.; Egidi, F.; Goings, J.; Peng, B.; Petrone, A.; Henderson, T.; Ranasinghe, D.; Zakrzewski, V. G.; Gao, J.; Rega, N.; Zheng, G.; Liang, W.; Hada, M.; Ehara, M.; Toyota, K.; Fukuda, R.; Hasegawa, J.; Ishida, M.; Nakajima, T.; Honda, Y.; Kitao, O.; Nakai, H.; Vreven, T.; Throssell, K.; Montgomery, J. A., Jr.; Peralta, J. E.; Ogliaro, F.; Bearpark, M. J.; Heyd, J. J.; Brothers, E. N.; Kudin, K. N.; Staroverov, V. N.; Keith, T. A.; Kobayashi, R.; Normand, J.; Raghavachari, K.; Rendell, A. P.; Burant, J. C.; Iyengar, S. S.; Tomasi, J.; Cossi, M.; Millam, J. M.; Klene, M.; Adamo, C.; Cammi, R.; Ochterski, J. W.; Martin, R. L.; Morokuma, K.; Farkas, O.; Foresman, J. B.; Fox, D. J.*Gaussian 16*, rev. B.01; Gaussian, Inc.: Wallingford, CT, 2016.
(140) Becke, A. D. Density-functional exchange-energy approximation with correct asymptotic behaviour. *Phys. Rev. A* **1988**, *38*, 3098−3100.
(141) Perdew, J. P. Density-functional approximation for the correlation energy of the inhomogeneous electron gas. *Phys. Rev. B* **1986**, *33*, 8822−8824.
(142) Wachters, A. J. H. Gaussian Basis Set for Molecular Wavefunctions Containing Third-Row Atoms. *J. Chem. Phys.* **1970**, *52*, 1033−1036.
(143) McLean, A. D.; Chandler, G. S. Contracted Gaussian basis sets for molecular calculations. 1. Second row atoms, Z = 11−18. *J. Chem. Phys.* **1980**, *72*, 5639−5648.
(144) Nemykin, V. N.; Hadt, R. G.; Belosludov, R. V.; Mizuseki, H.; Kawazoe, Y. Influence of Molecular Geometry, Exchange-Correlation Functional, and Solvent Effects in the Modeling of Vertical Excitation Energies in Phthalocyanines Using Time-Dependent Density Functional Theory (TDDFT) and Polarized Continuum Model TDDFT Methods: Can Modern Computational Chemistry Methods Explain Experimental Controversies? *J. Phys. Chem. A* **2007**, *111*, 12901−12913.
(145) Belosludov, R. V.; Nevonen, D.; Rhoda, H. M.; Sabin, J. R.; Nemykin, V. N. Simultaneous Prediction of the Energies of Qx and Qy Bands and Intramolecular Charge- Transfer Transitions in Benzoannulated and Non- Peripherally Substituted Metal- Free Phthalocyanines and Their Analogues: No Standard TDDFT Silver Bullet Yet. *J. Phys. Chem. A* **2019**, *123*, 132−152.
(146) Nemykin, V. N.; Basu, P. Comparative theoretical investigation of the vertical excitation energies and the electronic structure of $[Mo^{V}OCl_4]^{-}$: influence of basis set and geometry. *Inorg. Chem.* **2003**, *42*, 4046−4056.
(147) Martynov, A. G.; Mack, J.; May, A. K.; Nyokong, T.; Gorbunova, Y. G.; Tsivadze, A. Yu Methodological Survey of Simplified TD- DFT Methods for Fast and Accurate Interpretation of UV- Vis-NIR Spectra of Phthalocyanines. *ACS Omega* **2019**, *4*, 7265−7284.
(148) Staroverov, V. N.; Scuseria, G. N.; Tao, J.; Perdew, J. P. Comparative assessment of a new nonempirical density functional: Molecules and hydrogen-bonded complexes. *J. Chem. Phys.* **2003**, *119*, 12129−12137.
(149) Tao, J. M.; Perdew, J. P.; Staroverov, V. N.; Scuseria, G. E. Climbing the density functional ladder: Nonempirical meta-generalized gradient approximation designed for molecules and solids. *Phys. Rev. Lett.* **2003**, *91*, 146401.
(150) Cohen, A. J.; Handy, N. C. Dynamic correlation,. *Mol. Phys.* **2001**, *99*, 607−615.

https://doi.org/10.1021/acs.inorgchem.2c03456
Inorg. Chem. 2022, 61, 20177−20199

(151) Boese, A. D.; Martin, J. M. L. Development of density functionals for thermochemical kinetics. *J. Chem. Phys.* **2004**, *121*, 3405−3416.
(152) Hamprecht, F. A.; Cohen, A.; Tozer, D. J.; Handy, N. C. Development and assessment of new exchange-correlation functionals,. *J. Chem. Phys.* **1998**, *109*, 6264−6271.
(153) Schmider, H. L.; Becke, A. D. Optimized density functionals from the extended G2 test set,. *J. Chem. Phys.* **1998**, *108*, 9624−9631.
(154) Zhao, Y.; Schultz, N. E.; Truhlar, D. G. Exchange-correlation functionals with broad accuracy for metallic and nonmetallic compounds, kinetics, and noncovalent interactions. *J. Chem. Phys.* **2005**, *123*, 161103.
(155) Zhao, Y.; Truhlar, D. G. The M06 suite of density functionals for main group thermochemistry, thermochemical kinetics, noncovalent interactions, excited states, and transition elements: two new functionals and systematic testing of four M06 functionals and twelve other functionals. *Theor. Chem. Acc.* **2008**, *120*, 215−241.
(156) Tomasi, J.; Mennucci, B.; Cammi, R. Quantum mechanical continuum solvation models. *Chem. Rev.* **2005**, *105*, 2999−3093.
(157) Tenderholt, A. L.*QMForge*, ver. 2.1; Standord University: Stanford, CA, 2011. https://qmforge.net/.
(158) *SAINT*, ver. 7.46A; Bruker AXS Inc.: Madison, WI, 1997−2007. *SADABS. Bruker Nonius Area Detector Scaling and Absorption Correction*, ver. 2.10; Bruker AXS Inc.: Madison, WI, 2003.
(159) Altomare, A.; Burla, M. C.; Camalli, G.; Cascarano, M.; Giacovazzo, C.; Guagliardi, A.; Moliterni, A. G. G.; Polidori, G.; Spagna, A. SIR97: A new tool for crystal structure determination and refinement. *J. Appl. Crystallogr.* **1999**, *32*, 115−119.
(160) Altomare, A.; Cascarano, G.; Giacovazzo, C.; Guagliardi, A. SIR92. *J. Appl. Crystallogr.* **1993**, *26*, 343−350.
(161) *SHELXTL*, ver. 5.1; Bruker AXS Inc.: Madison, WI, 1997.
(162) Macrae, C. F.; Bruno, I. J.; Chisholm, J. A.; Edgington, P. R.; McCabe, P.; Pidcock, E.; Rodriguez-Monge, L.; Taylor, R.; van de Streek, J.; Wood, P. A. Mercury CSD 2.0 − new features for the visualization of crystal structures. *J. Appl. Crystallogr.* **2008**, *41*, 466−470.
(163) Fenn, T. D.; Ringe, D.; Petsko, G. A. POVScript+: A program for model and data visualization using persistence of vison ray-tracing. *J. Appl. Crystallogr.* **2003**, *36*, 944−947.

https://doi.org/10.1021/acs.inorgchem.2c03456
Inorg. Chem. 2022, 61, 20177−20199